2015

DETERMINATION OF ISOLATOR TRANSFER MATRIX AND INSERTION LOSS WITH APPLICATION TO SPRING MOUNTS

Shishuo Sun
University of Kentucky, sunshishuo@gmail.com

STUDENT AGREEMENT:

I represent that my thesis or dissertation and abstract are my original work. Proper attribution has been given to all outside sources. I understand that I am solely responsible for obtaining any needed copyright permissions. I have obtained needed written permission statement(s) from the owner(s) of each third-party copyrighted matter to be included in my work, allowing electronic distribution (if such use is not permitted by the fair use doctrine) which will be submitted to UKnowledge as Additional File.

I hereby grant to The University of Kentucky and its agents the irrevocable, non-exclusive, and royalty-free license to archive and make accessible my work in whole or in part in all forms of media, now or hereafter known. I agree that the document mentioned above may be made available immediately for worldwide access unless an embargo applies.

I retain all other ownership rights to the copyright of my work. I also retain the right to use in future works (such as articles or books) all or part of my work. I understand that I am free to register the copyright to my work.

REVIEW, APPROVAL AND ACCEPTANCE

The document mentioned above has been reviewed and accepted by the student's advisor, on behalf of the advisory committee, and by the Director of Graduate Studies (DGS), on behalf of the program; we verify that this is the final, approved version of the student's thesis including all changes required by the advisory committee. The undersigned agree to abide by the statements above.

Shishuo Sun, Student

Dr. David W. Herrin, Major Professor

Dr. Haluk E. Karaca, Director of Graduate Studies

DETERMINATION OF ISOLATOR TRANSFER MATRIX AND INSERTION LOSS WITH APPLICATION TO SPRING MOUNTS

THESIS

A thesis submitted in partial fulfillment of the
requirements for the degree of Master of Science
in Mechanical Engineering in the College of Engineering
at the University of Kentucky

By

Shishuo Sun

Lexington, Kentucky

Director: Dr. David W. Herrin, Professor of Mechanical Engineering

Lexington, Kentucky

2015

ABSTRACT OF THESIS

DETERMINATION OF ISOLATOR TRANSFER MATRIX AND INSERTION LOSS WITH APPLICATION TO SPRING MOUNTS

Transmissibility is the most common metric used for isolator characterization. However, engineers are becoming increasingly concerned about energy transmission through an isolator at high frequencies and how the compliance of the machine and foundation factor into the performance. In this study, the transfer matrix approach for isolator characterization is first reviewed. Two methods are detailed for determining the transfer matrix of an isolator using finite element simulation. This is accomplished by determining either the mobility or impedance matrix for the isolator and then converting to a transfer matrix. One of the more useful metrics to characterize the high frequency performance of an isolator is insertion loss. Insertion loss is defined as the difference in transmitted vibration in decibels between the unisolated and isolated cases. Insertion loss takes into account the compliance on the source and receiver sides. Accordingly, it has some advantages over transmissibility which is a function of the damping and mounted resonant frequency. A static analysis is to preload the isolator so that stress stiffening is accounted for. This is followed by modal and forced response analyses to identify the transfer matrix of the isolator. In this paper, the insertion loss of spring isolators is examined as a function of several geometric parameters including the spring diameter, wire diameter, number of active coils, and height. Results demonstrate how modifications to these parameters affect the insertion loss and the first surge frequency.

KEYWORDS: Vibration Isolation, Four Pole Parameters, Insertion Loss, Spring Isolator, Finite Element Simulation

Shishuo Sun
Student's Signature

18th December, 2015
Date

DETERMINATION OF ISOLATOR TRANSFER MATRIX AND INSERTION LOSS WITH APPLIACTION TO SPRING MOUNTS

By

Shishuo Sun

Dr. David W. Herrin
Director of Thesis

Dr. Haluk E. Karaca
Director of Graduate Studies

18th December, 2015
Date

ACKNOWLEDGEMENTS

Foremost, I would like to express my sincere gratitude to my advisor Professor David Herrin for the continuous support and help in my graduate study and research, for his patience, motivation, enthusiasm, and knowledge. His guidance helped me of research and writing of this thesis. I am also grateful to Professor Tingwen Wu, for his encouragement and great help on my research.

I would also like to thank Professor John Baker for being my committee member and providing great help on my research work for this paper.

I would like to thank my fellows and friends in the Vibro-Acoustics group: Huangxing Chen, Keyu Chen, Gong Cheng, Rui He, Xin Hua, Quentin Hunsucker, Jiazhu Li, Jundong Li, Wanlu Li, Caoyang Li, Weiyun Liu, Kangping Ruan, Peng Wang, Ruimeng Wu, Yitian Zhang, Nan Zhang and Limin Zhou, for all the great times we had.

Last but not the least, I would like to thank my family for their support and love.

TABLE OF CONTENTS

LIST OF TABLES

LIST OF FIGURES

CHAPTER 1 INTRODUCTION

1.1 Introduction

Noise is undesirable in vehicles and machines. High noise levels have adverse health consequences and are an annoyance. Accordingly, noise and vibration levels must often be minimized to meet consumer expectations or legal requirements and measures are taken to reduce or attenuate the noise. Noise is primarily classified according to its path. The vibro-acoustic path refers to noise that is produced by vibration. Structural vibration drives the contiguous air producing sound waves. Alternatively, noise is often produced by flow or combustion which is commonly referred to as aero-acoustic. Common aero-acoustic sources include fan and wind noise. Frequently, measures must be taken to reduce both paths, vibro- and aero-acoustic, for a given vehicle or machine.

The focus of this thesis is on the vibro-acoustic path. In general, vibro-acoustic energy propagation can be considered using a source-path-receiver concept as illustrated in Figure 1.1. Sources include prime movers, including engines, motors, compressors, pumps, and fans, produce vibrations which propagate through connected structures. Paths are structureborne and airborne energy pathways from the source to a receiver point and are sometimes represented as transfer functions between the source and the receiver. Frequently, vibrations travel from the prime mover to connected components and panels. Hence, noise will be radiated from the prime movers but also from the connected panels. Connected panels often represent the major pathway for noise propagation due to their large area.

Noise resulting from vibration can be minimized by reducing the area of the vibrating surface. Accordingly, noise issues frequently develop when a prime mover is attached to a panel or other component with large surface area. In that case, the panel acts as a sound board increasing the generated noise. Though it is recommended to minimize vibration levels at the source, it is often unfeasible to sufficiently reduce the vibration level to an acceptable level. In that case, it is

recommended to introduce an impedance mismatch into the path so that vibrational energy does not propagate from the source to other components. This is commonly achieved by positioning isolators or mounts between the sources and neighboring components.

Figure 1.1 The general model used to characterize the noise control or vibration problem.

Vibration isolators are widely used for vehicles, heavy equipment, climate control equipment in buildings, and other applications. Typical vibration isolators (as shown in Figure 1.2) employ a helical spring to provide stiffness, and an elastomeric layer (such as rubber or neoprene) to provide additional damping. Other types use a solid elastomeric element which is not so stiff and provides damping.

The effectiveness of a vibration isolator is determined by its dynamic properties and the properties of the dynamic system. Often, the mass of the isolator is neglected and the isolator is modeled as a frequency dependent spring and damper termed a dynamic stiffness.

As overall noise levels in vehicles and machinery are reduced, higher frequency noise which had been masked in the past by other sources of noise is becoming increasingly important. Specifically, surge frequencies or modes arise in the isolator itself. In that case, a dynamic stiffness model is insufficient because the mass of the isolator is neglected and associated modal behavior is ignored.

The metric that has been most commonly used to assess isolator performance is known as the transmissibility or transmissibility ratio (Inman, 2001). It is defined as the ratio between magnitudes for the forces or displacements on the input and output sides of an isolator. While worthwhile, transmissibility is a property of the isolator, and source or receiver mass. However, transmissibility does not take

into account the compliance of source or receiver sides. In addition, transmissibility has usually, though not exclusively, been used with the dynamic stiffness model for an isolator.

Figure 1.2 Typical commercially available vibration isolators.

Noise and vibration engineers are now moving towards more complete descriptions of the isolator performance where isolators are modeled using a state variable matrix termed a transfer matrix. The transfer matrix is frequency dependent and relates the forces and vibrations on one side of the isolator to those on the other side (Dickens, 1994, Dickens, 1995, Dickens, 1998, Dickens, 2000, Norwood, 1998, Snowdon, 1971 and Snowdon, 1979). The transfer matrix terms, which are sometimes called four-pole parameters, incorporate the modal behavior of the isolator.

The metric that is commonly used with the transfer matrix approach is isolator effectiveness. Isolator effectiveness is the ratio of the vibration on the receiver side with a rigid attachment to that with the isolator installed. When expressed in decibels, isolator effectiveness is termed an insertion loss which is analogous to the case for mufflers and silencers. Isolator effectiveness has the added of advantage of being able to incorporate the compliance of the source and the foundation along with modal interactions between the isolator and connected structures.

This thesis will focus on the transfer matrix approach. This will be further detailed and discussed in the later chapter. One advantage of the transfer matrix approach is that more representative metrics can be used to assess effectiveness of an isolator. On the other hand, the transfer matrix of an isolator is primarily a property of the isolator alone.

1.2 Objective

The objective of this thesis is to show how simulation can be used to determine the transfer matrix of an isolator. It is shown that isolator transfer matrices can be determined using finite element analysis by first determining either the impedance or mobility matrix. It is shown that both approaches are comparable. The transfer matrix method is then used to determine isolator insertion loss. Results are compared to direct calculation using frequency based substructuring with good agreement. As an example, the approach is used to determine the insertion loss of a spring isolator placed between two plates. The approach is also illustrated for a construction cab and it is shown that insertion loss has limited value for the multi-isolator case.

The research then focuses on coiled spring isolators. Specifically, the geometric parameters which determine the stiffness and mass of the isolator including the spring diameter, wire diameter, number of active coils, and spring height are varied. It is demonstrated how these factors affect the insertion loss and the first surge frequency.

1.3 Organization

This thesis is organized in to five chapters. The first chapter serves to introduce the research topic and provide an overview of the research provided herein.

Chapter 2 provides some general background reviewing the traditional characterization of vibration isolators as well as methods of measurement. It includes detailed definitions for the transmissibility, dynamic stiffness and isolator

effectiveness. In addition, it looks at transfer matrix theory and how the various elements like masses, springs, and dampers may be modeled.

In Chapter 3, the impedance and mobility methods for determining the transfer matrix of an isolator using finite element simulation are described. Use of the results to find the isolator insertion loss is demonstrated for a coiled spring isolator between two plates. The effect of making changes to the structural impedance on the machine side of isolator by adding or removing ribs is then examined.

In Chapter 4, the transfer matrix of a spring isolator is determined using finite element simulation and the insertion loss is then determined using assumed values for the compliance on the source and receiver sides. The effect of different geometric parameters on insertion loss and the first surge frequency for steel coil springs is then examined.

Chapter 5 summarizes the current work and includes recommendations for future research.

CHAPTER 2 BACKGROUND

The most obvious way to reduce vibration is at the source. However, it is normally not possible to reduce the vibration to an acceptable level. In that case, the typical means of noise and vibration control is to isolate the vibration source from the system. This is most easily achieved by using vibration isolation between the vibrating components and neighboring components. There are several different ways to characterize the properties of isolators which are described in this chapter.

2.1 Dynamic Stiffness

The most common way to characterize an isolator is to model it as a dynamic stiffness. The dynamic stiffness (k_d) can be expressed as

$$k_d = \frac{j\omega F}{v_1 - v_2} \tag{2.1}$$

where F is the dynamic force, v_1 and v_2 are the vibration on either side of the isolator, and ω is the angular frequency in rad/sec. The dynamic force (F) is assumed to be equal and opposite on each side of the isolator so inertial effects of the isolator are not considered. For simplicity, the dynamic stiffness is often assumed to be independent of frequency. However, the dynamic stiffness can be complex, including both stiffness and damping terms, and frequency dependent for the general case. The measurement for dynamic stiffness is generally divided into direct and indirect methods (ISO, 1997 and ISO, 2002).

2.2 Transmissibility

Transmissibility or transmissibility ratio is the metric that is most commonly used for assessing isolator performance (Dickens, 1998). It is defined as the ratio between magnitude of either the displacements or forces on the input and output sides of an isolator, and may be defined in terms of either displacements or forces. The traditionally used description of transmissibility is that it is usually

measured by supporting a mass on the vibration isolator, which is in turn supported on a rigid foundation, to form a single degree of freedom system.

Inman (2001) summarizes these concepts well. There are two commonly used descriptions of vibration transmissibility. In the first, the foundation is isolated from the vibrating source as illustrated in Figure 2.1. The mass is forced and the foundation is blocked. Alternatively, the component can be isolated from a moving foundation as shown in Figure 2.2. In this case, an enforced displacement is applied to the foundation and the component is considered as a receiver mass. Inman shows that the equations are the same for reducing the force or vibration transmission though they represent different isolation problems.

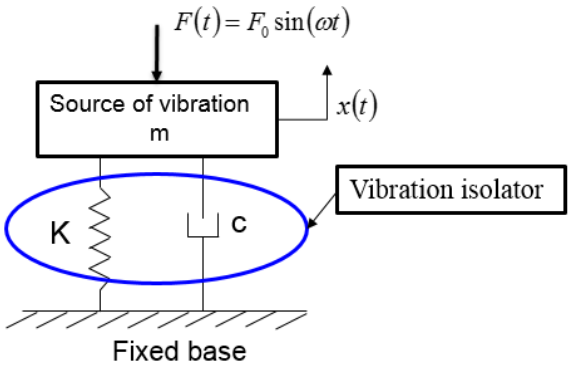

Figure 2.1 Schematic illustrating force transmissibility problem (Inman, 2001).

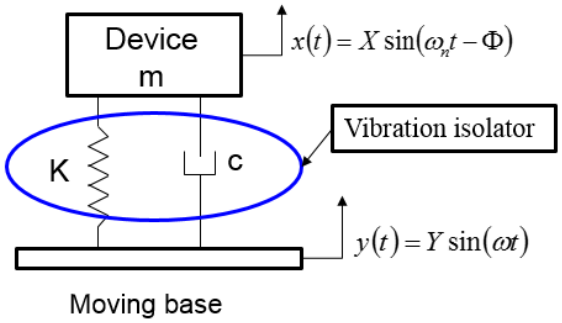

Figure 2.2 Schematic illustrating displacement transmissibility problem (Inman, 2001).

For the single degree of freedom system shown in Figures 2.1 and 2.2, m, k, and c are the mass, stiffness, and damping respectively. It is assumed that these

quantities are constant. The transmissibility ratio ($T.R.$), by either the force or vibration definition, can be expressed as

$$T.R. = \frac{F_T}{F_0} = \frac{X}{Y} = \sqrt{\frac{1 + (2\xi r)^2}{(1 - r^2)^2 + (2\xi r)^2}} \tag{2.2}$$

Where ξ is the damping ratio and r is the frequency ratio. These can be expressed as

$$\xi = \frac{c}{2m\omega_n} \tag{2.3}$$

$$r = \frac{\omega}{\omega_n} \tag{2.4}$$

where $\omega_n = \sqrt{k/m}$ is the natural frequency of the system.

Figure 2.3 shows the relationship of transmissibility ratio $T.R.$ and the frequency ratio r for different damping ratios (ξ). When the frequency ratio r is greater than $\sqrt{2}$, the magnitude of response is smaller than the input disturbance which implies that vibration isolation occurs. If r is less than $\sqrt{2}$, then the response is larger than the input disturbance and the isolator amplifies the force or vibration.

The damping ratio significantly affects the amplitude of vibration. Near the resonant frequency of the isolator, large damping ratios decrease the amount of amplification. However, vibration isolation systems should be designed to be used for frequency ratios (r) greater than $\sqrt{2}$. Figure 2.4 shows a close up on the region for r exceeding $\sqrt{2}$. In this region, the transmissibility ratio is reduced for small damping ratios (ξ).

According to Figure 2.4, r is increased for a fixed ω, the value of $T.R.$ decreases. This corresponds to increasing the mass or decreasing the stiffness of the isolator, as shown previously. As damping is increased for a fixed r, the value of $T.R.$ increases, so that low damping is often used. Figure 2.4 illustrates that for

frequency ratios (r) exceeding 3 with small damping ratios (ξ) below 0.02, $T.R.$ is not significantly affected by decreasing damping further.

Because the internal damping of most springs is less than 0.01, $(2\xi r)^2$ is small and can be neglected in Equation (2.2) for preliminary vibration isolator design. Then Equation (2.2) can be simplified as

$$T.R. = \frac{1}{r^2 - 1} \tag{2.5}$$

where it is assumed that $r > 3$.

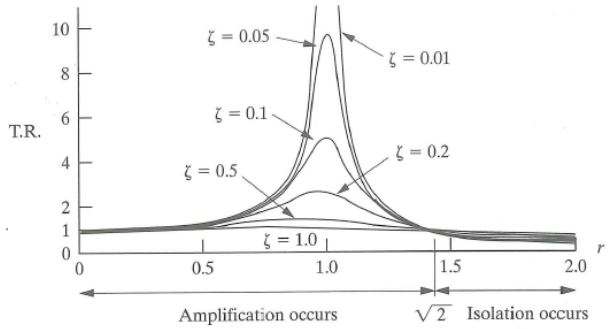

Figure 2.3 Plot of the transmissibility ratio for different damping ratios and the frequency ratios (Inman, 2001).

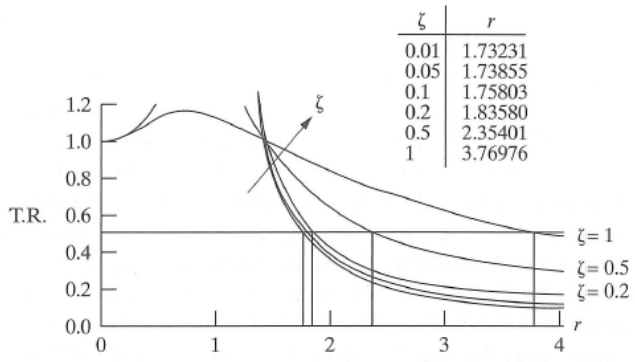

Figure 2.4 Force or displacement transmissibility for a viscously damped single degree of freedom system, focusing on the vibration isolation region (Inman, 2001).

Inman (2001) details a procedure for selecting isolators based upon the constant dynamic stiffness model. The static deflection of a spring can be expressed as

$$\Delta_{static} = \frac{mg}{k} \tag{2.6}$$

where m is the mass of the machine and g is the acceleration due to gravity. In order to quantify the performance of the vibration isolator, the reduction in transmissibility (R) is introduced and defined as

$$R = 1 - T.R. \tag{2.7}$$

Assuming that the excitation is harmonic and given in revolutions per minute (n), the input rpm (n) can be expressed in terms of the reduction in transmissibility (R) and static deflection as

$$n = \frac{30}{\pi}\sqrt{\frac{g(2-R)}{\Delta_{static}(1-R)}} = 29.9093\sqrt{\frac{2-R}{\Delta_{static}(1-R)}} \tag{2.8}$$

by combining Equations (2.5, 2.6, and 2.7). Equation (2.8) can be used to generate design curves for isolators. Taking the logarithm of Equation (2.8) yields

$$\log_{10} n = \frac{1}{2}\log_{10} \Delta_{static} + \log_{10}\left(29.9093\sqrt{\frac{2-R}{1-R}}\right) \tag{2.9}$$

which is a straight line on a log-log plot as a function of R. Design curves are plotted in Figure 2.5.

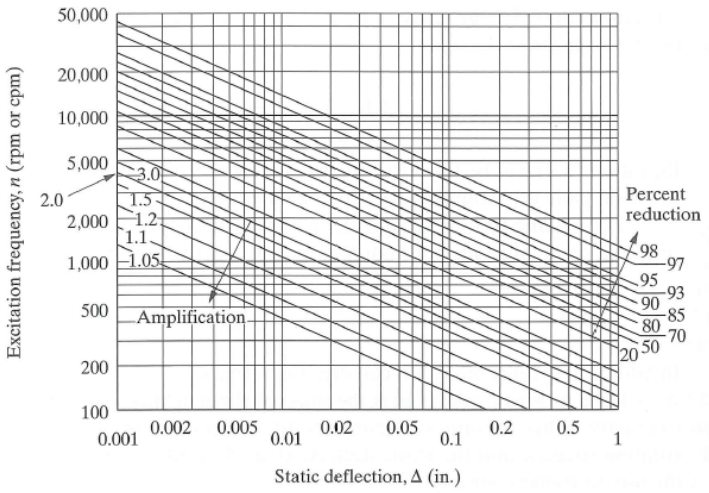

Figure 2.5 Design curves consisting of plots of speed in rpm versus static deflection for various values of percent reduction in transmitted force (Inman, 2011).

As an example, suppose that a 3 kg motor operates at 5000 rpm and it is desired that the force be reduced by 95% at the base. Using Figure 2.5, it can be seen that a static deflection of 0.003 in (or 0.762 mm) is desired. The spring stiffness can then be found via

$$k = \frac{mg}{\Delta_{static}} = \frac{(3\ kg)(9.8\ m/s^2)}{0.000762\ m} = 38{,}582\ N/m \tag{2.10}$$

Inman (2001) recommends that the choice of clearance should be more than twice the static deflection so that the spring has enough space to extend and compress and provide the requisite vibration isolation.

This analysis is based on using the simplified relationship for transmissibility ratio ($T.R.$) given in Equation (2.5) which assumes a single degree of freedom system and small damping. At higher frequencies, a coil spring will have additional internal resonances at which the isolator will effectively transmit vibration. Sometimes an elastomer layer is placed between the spring and its support to add higher frequency damping in commercial isolators. In order to simulate these higher frequency effects, a more complete model of an isolator is desired. Several authors have suggested using a transfer matrix model of an isolator which includes the modal behavior of the isolator (Dickens, 2000, Forrest, 2006,

Gardonio, 2000, Norwood, 1998, Snowdon, 1965, Snowdon, 1968 and Soliman, 1968).

2.3 Transfer Matrix Model of Isolator

Molloy (1957) appears to have originally suggested developing a two-port network for mechanical systems. The theory is virtually identical to that described by Munjal (1987) for acoustical systems, with the variables being acoustical pressure and volume velocity. After which, Snowdon (1971) further developed the theory and applied it to vibration isolation. Snowdon (1971) proposed and developed a testing apparatus to measure the four-pole parameters of vibration isolators. Snowdon basically used the Schloss' (1965) test rig, which is shown in Figure 2.6. Schloss used the test rig to measure the blocked transfer impedance and blocked driving point impedance of vibration isolators under static load. Dickens and Norwood (1998) proposed a two-mass method to measure the four-pole parameters of a vibration isolator, by using two different floating masses. The approach was general and applicable to asymmetric isolators under a static pre-load.

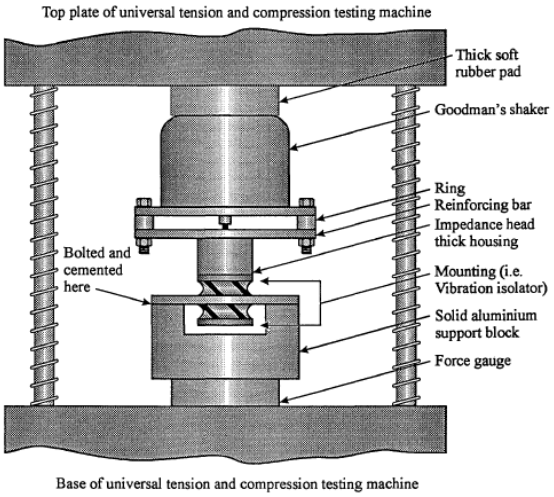

Figure 2.6 Proposed test rig of Snowdon, after Schloss. (Dickens and Norwood, 1998).

Kim and Singh (2001, 2003) have researched elastometric isolators using a more sophisticated mobility matrix approach. In their efforts, a multi-axial model was used for the isolator and analytical results were compared with measurement. In addition, they developed an approach for estimating the mobility matrix via measurement. However, the approach used did not take into account the preload on the isolator.

Transfer matrix theory is reviewed in the discussion which follows. A vibration isolator is modeled as a linear system, where the dynamic force and velocity at its input side are denoted by F_1 and v_1 respectively, and at its output side by F_2 and v_2 respectively. Figure 2.7 shows a schematic of an isolator with forces (F_1 and F_2) and velocities (v_1 and v_2) identified along with the sign convention. The input and output sides are denoted by the indices 1 and 2 respectively. The forces and vibration on either side can be related to one another using the expression

$$\begin{Bmatrix} F_1 \\ v_1 \end{Bmatrix} = \begin{bmatrix} a_{11} & a_{12} \\ a_{21} & a_{22} \end{bmatrix} \begin{Bmatrix} F_2 \\ v_2 \end{Bmatrix} \tag{2.11}$$

where a_{11}, a_{12}, a_{21}, and a_{22} are the transfer matrix terms or four-pole parameters. These transfer matrix terms are complex and frequency dependent.

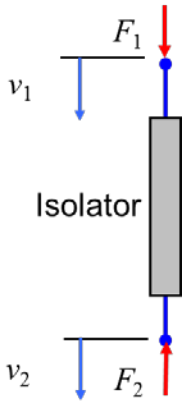

Figure 2.7 Schematic illustrating mount with force and velocity variables.

If F_2 and v_2 are considered as the input port and F_1 and v_1 as the output port, F_2 and v_2 can be solved with respect to F_1 and v_1. F_2 and v_2 can be expressed as

$$\begin{Bmatrix} F_2 \\ v_2 \end{Bmatrix} = \frac{1}{\Delta}\begin{bmatrix} a_{22} & -a_{12} \\ -a_{21} & a_{11} \end{bmatrix}\begin{Bmatrix} F_1 \\ v_1 \end{Bmatrix} \quad (2.12)$$

where Δ is the determinant of the transfer matrix and can be expressed as

$$\Delta = a_{11}a_{22} - a_{12}a_{21} \quad (2.13)$$

Assuming that the Rayleigh reciprocity theorem in the form of Maxwell's law of reciprocal deflections applies to the system (Dickens and Norwood, 1998), it follows that the transfer impedance or mobility between any two ports is independent of which port is treated as the input or output. Accordingly, the two blocked transfer mobilities are equal which gives rise to the relationship

$$\left.\frac{v_1}{F_2}\right|_{v_2=0} = \left.\frac{v_2}{F_1}\right|_{v_1=0} \quad (2.14)$$

By combining Equations (2.11, 2.12, and 2.14), it can be shown that the determinant is equal to unity. This can be expressed mathematically as

$$\Delta = a_{11}a_{22} - a_{12}a_{21} = 1 \quad (2.15)$$

A symmetric isolator is bidirectional meaning that either side can be used as input or output. Secondly, the isolator properties remain unchanged if the input and output sides are interchanged. By inserting Equation (2.15) into Equation (2.12), it can be shown that

$$\begin{Bmatrix} F_2 \\ v_2 \end{Bmatrix} = \begin{bmatrix} a_{22} & a_{12} \\ a_{21} & a_{11} \end{bmatrix}\begin{Bmatrix} F_1 \\ v_1 \end{Bmatrix} \quad (2.16)$$

The four-pole parameters provided by Equations (2.11) and (2.16) should be identical. Accordingly, it can be seen that

$$a_{11} = a_{22} \quad (2.17)$$

Given Equations (2.15) and (2.17), it is evident that there are only two independent transfer matrix terms for a symmetric isolator.

If the output is blocked (i.e., $v_2 = 0$), a_{11} and a_{21} can be expressed as

$$a_{11} = \left.\frac{F_1}{F_2}\right|_{v_2=0} \tag{2.18}$$

and

$$a_{21} = \left.\frac{v_1}{F_2}\right|_{V_2=0} \tag{2.19}$$

respectively.

Alternatively, if the output side is unrestrained and is free to vibrate (i.e. $F_2 = 0$), a_{12} and a_{22} can be written as

$$a_{12} = \left.\frac{F_1}{v_2}\right|_{F_2=0} \tag{2.20}$$

and

$$a_{22} = \left.\frac{v_1}{v_2}\right|_{F_2=0} \tag{2.21}$$

respectively.

Equations (2.18) through (2.21) were posited by Snowdon (1979). Using either the blocked (Equations 2.18 and 2.19) or unforced (Equations 2.20 and 2.21) assumptions, Equations (2.15) and (2.17) can be used to solve for the remaining two transfer matrix terms for a symmetric isolator. While the second case is experimentally convenient, it is not allowable for the determination of the vibration isolator under static load, and therefore the properties measured in this way will not be representative of those for the installed vibration isolator. Accordingly, the approach for measuring the transfer matrix terms of a pre-loaded symmetric isolator depends on a blocked output arrangement that measures F_1, v_1 and F_2 with $v_2 = 0$.

Asymmetric vibration isolators do not have the same behavior if the input and output sides are interchanged. For asymmetric vibration isolators, Equation (2.17) is no longer appropriate and additional information is required. Snowdon (1979) proposed reversing the vibration isolator in the test rig so that the input and output ends are interchanged. Hence, the vibration isolator is tested in both the normal and reversed positions. A schematic of the testing setup is shown in Figure 2.8.

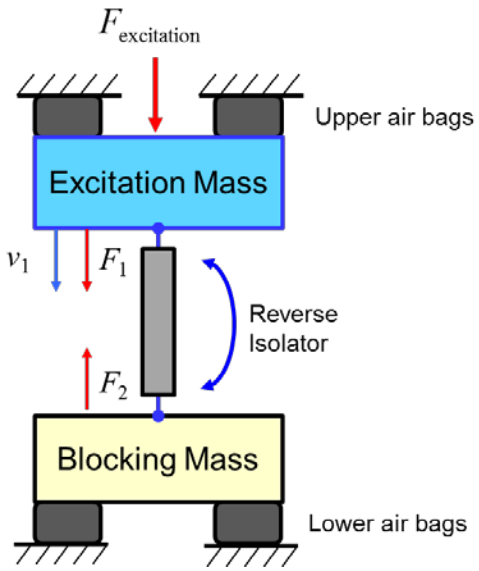

Figure 2.8 The test layout of a linear asymmetric isolator.

The input force and velocity for the reversed configuration are denoted by F_{1r} and v_{1r} on the input side, and F_{2r} and v_{2r} on the output side. The reversed configuration transfer matrix can be expressed as

$$\begin{Bmatrix} F_{1r} \\ v_{1r} \end{Bmatrix} = \begin{bmatrix} a_{22} & a_{12} \\ a_{21} & a_{11} \end{bmatrix} \begin{Bmatrix} F_{2r} \\ v_{2r} \end{Bmatrix} \tag{2.22}$$

For the blocked situation, $v_{2r} = 0$ yielding

$$a_{22} = \left. \frac{F_{1r}}{F_{2r}} \right|_{v_{2r}=0} \tag{2.23}$$

and

$$a_{21} = \left.\frac{v_{1r}}{F_{2r}}\right|_{v_{2r}=0} \tag{2.24}$$

Equation (2.23) provides the additional relationship needed to determine a_{22} and equation (2.24) can be used to experimentally check the value of a_{21}. This method has been termed the blocked reversal method (Snowdon, 1979).

In a similar manner, the reversing the isolator may be applied to the unblocked situation as well. In that case, Equations (2.10), (2.15) and (2.22) are combined together and the transfer matrix terms are written as

$$a_{12} = \frac{F_1 F_{1R} - F_2 F_{2R}}{v_1 F_{2R} + v_{2R} F_1} \tag{2.25}$$

$$a_{11} = \frac{F_1 - a_{12} v_2}{F_2} \tag{2.26}$$

$$a_{22} = \frac{F_2 + a_{12} v_1}{F_1} \tag{2.27}$$

$$a_{21} = \frac{v_1 - a_{22} v_2}{F_2} \tag{2.28}$$

This method is called the unblocked reversal method (Snowdon, 1979), and requires measurement of the input and output forces and velocities in normal and reversed configurations.

The blocked reversal method is generally preferred because it does not require the measurement of the output velocity. Both methods of reversing the vibration isolator in the test rig assume that the vibration isolator is bi-directional and it may be operated with its input and output sides interchanged. If the isolator operates in only a single direction and is irreversible, the above approach is not applicable.

Dickens and Norwood (2001) proposed and developed a two-mass method for measuring the four-pole parameters of uni-directional asymmetric vibration

isolators under static load. The two-mass method may be applied to uni-directional asymmetric isolators as well as the other isolators mentioned above.

Consider a uni-directional asymmetric isolator being tested under static load in the vibration isolator test facility and suppose that it is tested with two blocking masses of different mass. The test configurations are identical except for the blocking masses. Let the two blocking masses be denoted as m_{21} and m_{22}, and let the corresponding forces and velocities be respectively denoted by the second subscripts 1 and 2. The four-pole parameters are assumed to be the same for both sets of data, and therefore the two matrix equations corresponding to equation (2.11) are

$$\begin{Bmatrix} F_{11} \\ v_{11} \end{Bmatrix} = \begin{bmatrix} a_{11}\, a_{12} \\ a_{21}\, a_{22} \end{bmatrix} \begin{Bmatrix} F_{21} \\ v_{21} \end{Bmatrix} \tag{2.29}$$

and

$$\begin{Bmatrix} F_{12} \\ v_{12} \end{Bmatrix} = \begin{bmatrix} a_{11}\, a_{12} \\ a_{21}\, a_{22} \end{bmatrix} \begin{Bmatrix} F_{22} \\ v_{22} \end{Bmatrix} \tag{2.30}$$

Combining the above two equation (2.29 and 2.30) yields

$$\begin{Bmatrix} F_{11} \\ v_{11} \\ F_{12} \\ v_{12} \end{Bmatrix} = \begin{bmatrix} F_{21} & v_{21} & 0 & 0 \\ 0 & 0 & F_{21} & v_{21} \\ F_{22} & v_{22} & 0 & 0 \\ 0 & 0 & F_{22} & v_{22} \end{bmatrix} \begin{Bmatrix} a_{11} \\ a_{12} \\ a_{21} \\ a_{22} \end{Bmatrix} \tag{2.31}$$

Solving for the four-pole parameters yields

$$\begin{Bmatrix} a_{11} \\ a_{12} \\ a_{21} \\ a_{22} \end{Bmatrix} = \frac{1}{F_{22}v_{21} - F_{21}v_{22}} \begin{bmatrix} -v_{22} & 0 & v_{21} & 0 \\ F_{22} & 0 & -F_{21} & 0 \\ 0 & -v_{22} & 0 & v_{21} \\ 0 & F_{22} & 0 & -F_{21} \end{bmatrix} \begin{Bmatrix} F_{11} \\ v_{11} \\ F_{12} \\ v_{12} \end{Bmatrix} \tag{2.32}$$

Equation (2.32) is only valid if

$$F_{22}v_{21} \neq F_{21}v_{22} \tag{2.33}$$

Additional equations for the force on the output sides can be expressed as

$$F_{21} = j\omega m_{21} v_{21} \tag{2.34}$$

and

$$F_{22} = j\omega m_{22} v_{22} \tag{2.35}$$

Then using equations (2.32, 2.34 and 2.35), the four-pole parameters are determined to be

$$a_{11} = \frac{1}{m_{21} - m_{22}} \left(\frac{m_{21} F_{11}}{F_{21}} - \frac{m_{22} F_{12}}{F_{22}} \right) \tag{2.36}$$

$$a_{12} = \frac{j\omega m_{21} m_{22}}{m_{21} - m_{22}} \left(\frac{F_{12}}{F_{22}} - \frac{F_{11}}{F_{21}} \right) \tag{2.37}$$

$$a_{21} = \frac{1}{m_{21} - m_{22}} \left(\frac{m_{21} v_{11}}{F_{21}} - \frac{m_{22} v_{12}}{F_{22}} \right) \tag{2.38}$$

$$a_{22} = \frac{j\omega m_{21} m_{22}}{m_{21} - m_{22}} \left(\frac{v_{12}}{F_{22}} - \frac{v_{11}}{F_{21}} \right) \tag{2.39}$$

The two blocking masses should be sufficiently different masses to provide different sets of data for substitution into Equation (2.32). The only assumption is that the four-pole parameters remain unchanged for the two blocking masses.

2.4 Isolator Effectiveness / Isolator Insertion Loss

Ungar and Dietrich (1966) recommended the use of isolator effectiveness (E) as a metric to assess the performance of a vibration isolator installed in a system. Effectiveness is defined as the ratio of the receiver amplitude for the rigidly attached and isolated cases and can be expressed as

$$E = \frac{v_f\big|_{rigid}}{v_f\big|_{isolated}} \tag{2.40}$$

where $v_f\big|_{rigid}$ and $v_f\big|_{isolated}$ are the unisolated and isolated vibrations respectively. Figure 2.9 shows a schematic of the two situations. If the isolator effectiveness is in decibels, it is referred to an isolator insertion loss and can be expressed as

$$IL = 20 \cdot \log_{10}|E| \tag{2.41}$$

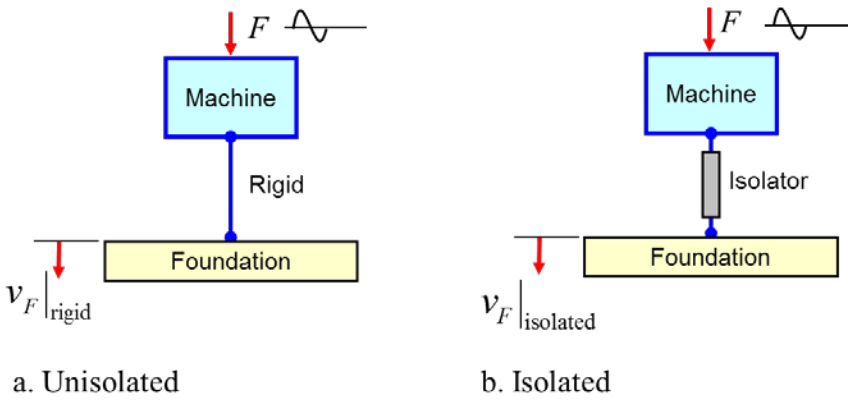

Figure 2.9 Schematic illustrating isolator insertion loss.

Let the driving point mobilities of the source and the foundation measured at the source and foundation connection points with vibration isolation, be H_1 and H_2 respectively as shown in Figure 2.10. The velocities at the source/vibration isolator and vibration isolator/foundation interfaces are v_1 and v_2 respectively. Let v_0 be the free velocity of the source at the connection point, i.e. the velocity without the vibration isolator connected to the source (Dickens, 1998). With the vibration isolator connected, the velocity changes to v_1, and by the principle of superposition, v_1 is the sum of the free velocity and the motion due to the resisting force of the vibration isolator, and therefore

$$v_1 = v_0 - Y_1 F_1 \tag{2.42}$$

Assuming that the free velocity of the foundation is zero, yields

$$v_2 = Y_2 F_2 \tag{2.43}$$

Solving Equations (2.11), (2.42) and (2.43) to obtain v_2 in terms of Y_1 and Y_2 gives

$$v_2 = \frac{v_0 Y_2}{a_{11}Y_1 + a_{12}Y_1Y_2 + a_{21} + a_{22}Y_2} \tag{2.44}$$

Consider the situation where the source and foundation are directly connected as shown in Figure 2.9.

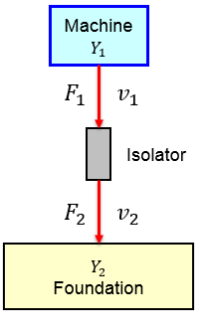

Figure 2.10 Schematic illustrating the driving point mobilities of the source and the foundation.

Let the velocities be denoted as above but primed and with a similar analysis it may be shown that

$$v_2{}' = \frac{v_0 Y_2}{Y_1 + Y_2} \tag{2.45}$$

From Equations (2.44), (2.45) and (2.40), it can also be expressed in terms of the four-pole parameters and the source and foundation mobilities as

$$E = \frac{a_{11}Y_1 + a_{12}Y_1Y_2 + a_{21} + a_{22}Y_2}{Y_1 + Y_2} \tag{2.46}$$

where Y_1 and Y_2 are the driving point mobilities of the source and the foundation measured at the source and foundation connection points respectively. This can also be expressed in terms of the source and foundation impedances as

$$IL = 20 \cdot \log_{10} \left| \frac{a_{11}Z_S + a_{12} + a_{21}Z_SZ_R + Z_R}{Z_s + Z_R} \right| \tag{2.47}$$

where Z_S and Z_R are the mechanical impedances at the isolator mounting points on source and receiver sides, respectively.

The mechanical impedances of the source and foundation (Z_S and Z_R respectively) can be determined by exciting the respective structure at the isolator attachment point and determining the response as illustrated in Figure 2.11. Accordingly,

$$Z_i = \frac{F_i}{v_i} \tag{2.48}$$

Where i refers to the appropriate attachment point on the source or receiver side. This impedance is easily determined using a structural finite element model or via measurement.

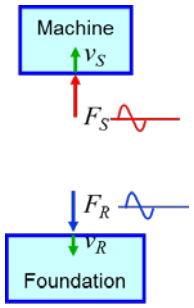

Figure 2.11 Schematic illustrating determination of impedances.

The concept of mobility will be introduced. The mobility of a system component is a complex, frequency dependent quantity, and is defined as the ratio of the velocity of response to force input (reciprocal of mechanical impedance), which can be expressed as

$$Y = v/F \tag{2.49}$$

The dynamic characteristics of the isolator then be presented in terms of its mobility parameters (Norwood, 1987 and Norwood, 1998). The effectiveness of an isolator is related to the relative mobilities of the isolated mass, the isolators themselves and the foundation or attached structures. If the isolator can be assumed to be massless, the isolator effectiveness can be expressed as

$$E = \left|1 + \frac{Y_I}{Y_S + Y_R}\right| \tag{2.50}$$

Where $M_I, M_S,$ and M_R are the isolator, source, and receiver mobilities, respectively (Ungar and Dietrich, 1966). For effective isolation, the mobility M_I must exceed the sum $Y_s + Y_r$ considerably, $|Y_I| \gg |Y_S + Y_R|$. Hence, to increase isolation effectiveness, one must either increase the isolator mobility or decrease the source and receiver mobilities.

For a symmetric vibration isolator, Norwood and Dickens (1998) showed that the isolator insertion loss can be expressed as

$$IL = 20 \cdot \log_{10} \left|a_{11} + \frac{a_{12} Y_1 H_2}{Y_1 + Y_2} + \frac{a_{21}}{Y_1 + Y_2}\right| \tag{2.51}$$

by combining Equations (2.17 and 2.46).

A simplified vibration isolation case is provided to demonstrate the characteristic properties of insertion loss. Figure 2.12 shows the insertion loss results for a rigid body mounted to a rigid foundation via a simple spring-damper isolator (indicated as “Rigid Foundation”). For comparison, the results with a compliant foundation (indicated as “Compliant Foundation”) are also shown. Notice that a compliant foundation reduces the insertion loss at higher frequencies. Wave propagation is included in the isolator in the third curve. Notice that there are a number of sharp troughs occurring at isolator resonances.

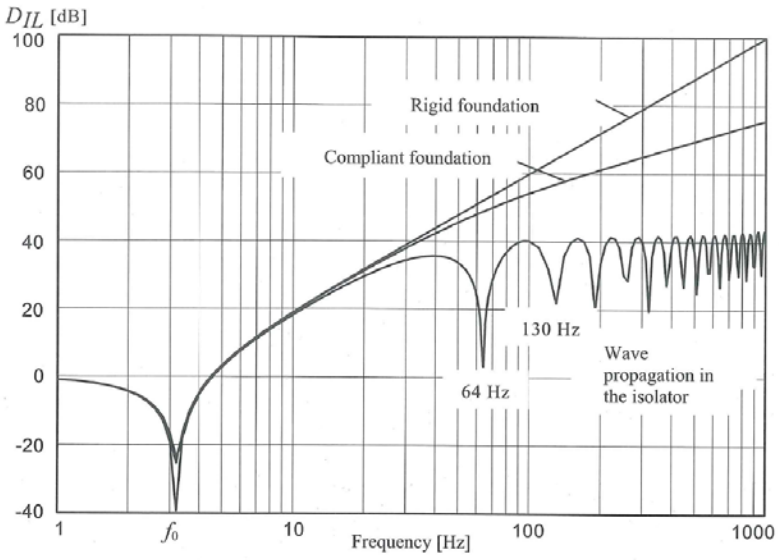

Figure 2.12 Insertion loss results illustrating the effect of wave propagation in isolator (Wallin et al., 2012).

2.5 Summary

The different models for isolators and associated metrics have been surveyed in this chapter. Isolators have traditionally been defined in terms of their dynamic stiffness which does not include inertial effects in the isolator. In that case, the metric that is most commonly used is the transmissibility which is defined as the ratio of the transmitted dynamic forces to the source dynamic force. Alternatively, transmissibility can be described in terms of the vibration. The primary drawback of using transmissibility is that the compliance on either side of the isolator is not included.

A more complete model of an isolator may be defined using the transfer matrix approach. This approach will included inertial effects and includes surge frequencies. When transfer matrices are used, isolator effectiveness or insertion loss is typically used to assess the isolator. Isolator effectiveness is defined as the ratio of the unisolated to isolated vibrations.

The next chapter will detail how the transfer matrix can be identified using structural finite element analysis. After which, the insertion loss calculation is demonstrated for a representative structure.

CHAPTER 3 DETERMINATION OF THE TRANSFER MATRIX FOR ISOLATORS USING SIMULATION WITH APPLICATION TO DETERMINING INSERTION LOSS

3.1 Introduction

Molloy (1957) first suggested using the transfer matrix approach to characterize isolators. Snowdon (1971) further developed the idea and derived a number of expressions for typical mass-spring-damper combinations. Dickens and Norwood (2001) developed an experimental approach for determining the transfer matrix or four-pole parameters of an isolator.

The work in this chapter focuses on developing the approaches to determine the transfer matrix of an isolator using finite element analysis. A static analysis is initially performed in order to include stress stiffening effects due to the static preload for the dynamic analysis that follows. After which, the structural modes of the isolator are determined by modal analysis which includes the effect of the pre-load. The transfer matrix can then be found by finding either the mobility or impedance matrix from two successive forced response analyses with different loading conditions.

This chapter will demonstrate the methodology which is applied to a spring isolator connecting two plates. One plate represents the machine side and the other massive plate can be considered as the foundation side. After which, the effect on insertion loss of adding ribs to the machine or source side is illustrated. In order to investigate the usefulness of the isolator insertion loss for multiple isolator cases, multiple isolators were applied between a construction cab and base foundation for a numerical simulation study.

3.2 Determination of the Four-Pole Parameters

The procedure for determining the four-pole parameters is summarized in Figure 3.1. First, a static finite element analysis is conducted to deal with the static pre-load. This analysis can be linear or nonlinear. The purpose of the analysis is to

update the stiffness matrix to include the pre-load (i.e., stress stiffening effects). If the pre-load does not significantly affect the structural modes of the isolator, the static analysis will be unnecessary.

This is followed by a second analysis to determine the structural modes (including the updated stiffness matrix). After which, two successive modal superposition forced response analyses are used to determine the four-pole parameters. All dynamic analyses assume that the loaded isolator behaves in a linear fashion and that displacements are small. All analyses were performed using ANSYS Workbench (ANSYS, 2014).

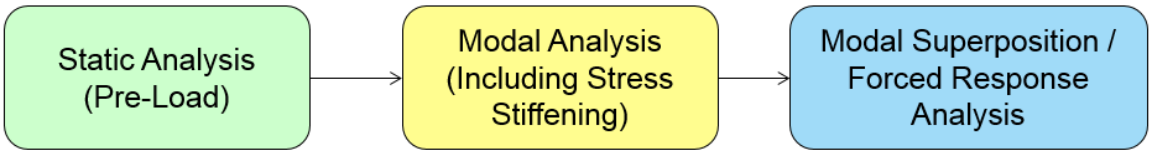

Figure 3.1 Flow chart illustrating analysis progression.

3.2.1 Mobility Matrix Approach

There are two convenient approaches for determining the transfer matrix. The first is a mobility matrix approach where the transfer matrix in Equation (2.11) is reconfigured as

$$\begin{Bmatrix} v_1 \\ v_2 \end{Bmatrix} = \begin{bmatrix} b_{11} & b_{12} \\ b_{21} & b_{22} \end{bmatrix} \begin{Bmatrix} F_1 \\ F_2 \end{Bmatrix} \tag{3.1}$$

where b_{11}, b_{12}, b_{21}, and b_{22} are mobility matrix terms. Two successive forced response analyses can be performed to determine the mobility matrix terms. The boundary conditions for the first and second analysis are

$$F_1 = 1; F_2 = 0 \tag{3.2}$$

and

$$F_1 = 0; F_2 = 1 \tag{3.3}$$

respectively. The mobility matrix terms (b_{11}, b_{12}, b_{21}, and b_{22}) can be determined from

$$b_{11} = \left.\frac{v_1}{F_1}\right|_{F_1=1;\, F_2=0} \tag{3.4}$$

$$b_{12} = \left.\frac{v_1}{F_2}\right|_{F_1=0;\, F_2=1} \tag{3.5}$$

$$b_{21} = \left.\frac{v_2}{F_1}\right|_{F_1=1;\, F_2=0} \tag{3.6}$$

$$b_{22} = \left.\frac{v_2}{F_2}\right|_{F_1=0;\, F_2=1} \tag{3.7}$$

where v_1, v_2, F_1, and F_2 are determined from analyses with the respective boundary conditions indicated.

The four-pole parameters can then be determined from the mobility matrix terms. This is expressed as

$$a_{11} = -\frac{b_{22}}{b_{21}} \tag{3.8}$$

$$a_{12} = \frac{1}{b_{21}} \tag{3.9}$$

$$a_{21} = b_{12} - \frac{b_{11}b_{22}}{b_{21}} \tag{3.10}$$

$$a_{22} = \frac{b_{22}}{b_{21}} \tag{3.11}$$

3.2.2 Impedance Matrix Approach

In a similar manner, the transfer matrix terms can be determined using an impedance matrix approach. In that case, Equation (2.11) can be rearranged as

$$\begin{Bmatrix} F_1 \\ F_2 \end{Bmatrix} = \begin{bmatrix} c_{11} & c_{12} \\ c_{21} & c_{22} \end{bmatrix} \begin{Bmatrix} v_1 \\ v_2 \end{Bmatrix} \tag{3.12}$$

where c_{11}, c_{12}, c_{21}, and c_{22} are the respective impedance matrix terms. Once again, two successive forced response analyses are conducted to determine the impedance matrix terms. The boundary conditions for the first and second analyses are

$$F_1 = 1; v_2 = 0 \tag{3.13}$$

and

$$F_2 = 1; v_1 = 0 \tag{3.14}$$

respectively. The impedance matrix terms (c_{11}, c_{12}, c_{21}, and c_{22}) can be determined from

$$c_{11} = \left.\frac{F_1}{v_1}\right|_{F_1=1;\, v_2=0} \tag{3.15}$$

$$c_{12} = \left.\frac{F_1}{v_2}\right|_{v_1=0;\, F_2=1} \tag{3.16}$$

$$c_{21} = \left.\frac{F_2}{v_1}\right|_{F_1=1;\, v_2=0} \tag{3.17}$$

$$c_{22} = \left.\frac{F_2}{v_2}\right|_{v_1=0;\, F_2=1} \tag{3.18}$$

where v_1, v_2, F_1, and F_2 are determined from analyses with the respective boundary conditions indicated.

The four-pole parameters can then be determined from the impedance matrix via

$$a_{11} = \frac{c_{11}}{c_{21}} \tag{3.19}$$

$$a_{12} = c_{12} - \frac{c_{11}c_{22}}{c_{21}} \tag{3.20}$$

$$a_{21} = \frac{1}{c_{21}} \tag{3.21}$$

$$a_{22} = -\frac{c_{22}}{c_{21}} \tag{3.22}$$

The primary difference between the two approaches is that the isolator is unconstrained if the mobility matrix approach is used, and alternately fixed on one side or the other if the impedance matrix approach is used.

3.3 Frequency Based Substructuring Approach

This thesis will focus on the transfer matrix approach. The transfer matrix approach can also be linked to frequency based substructuring (FBS) sometimes referred to as transfer path analysis (TPA) (W. Hendricx and D. Vandenbroeck, 1992, M. H. A. Janssens et al., 1999, T. C. Lim and G. C. Steyer, 1992, P.J. G. van der Linden and J. Fun, 1993, D. de Vis et al., 1992 and K. Wyckaert and H. Van der Auweraer, 1995).

In the case of FBS, isolators are commonly modeled as a dynamic stiffness if inertia effects can be neglected. However, the isolator is more properly defined as a separate dynamic system defined by the transfer functions between different isolator sides. The transfer functions can be expressed in terms of the transfer matrix term (four-pole parameters).

The transfer functions can be expressed in terms of the transfer matrix terms as

$$\frac{v_1}{F_1} = \frac{a_{22}}{a_{12}} \tag{3.23}$$

$$\frac{v_1}{F_2} = a_{21} - a_{22}\frac{a_{11}}{a_{12}} \tag{3.24}$$

$$\frac{v_2}{F_1} = -\frac{a_{11}}{a_{12}} \tag{3.25}$$

$$\frac{v_2}{F_2} = -\frac{a_{22}}{a_{21}} \tag{3.26}$$

All FBS analyses were performed using LMS Virtual.Lab in this chapter (LMS Virtual.Lab, 2014).

3.4 Example Case – Simple Spring Isolator

The procedures described above were used to determine the transfer matrix for a simple spring isolator. The diameter of the isolator and spring wire were 70 mm and 5 mm respectively, and the shear modulus was 76.9 GPa. There were approximately 4 active turns. The spring stiffness can be determined from

$$k = \frac{Gd^4}{8nD^3} \tag{3.27}$$

where G is the shear modulus, d is the diameter of the spring wire, D is the diameter of the spring, and n is the number of active turns. The static stiffness determined using finite element analysis was 4460 N/m, which compared well (within 2%) with 4380 N/m determined using Equation (3.27).

An 85 N pre-load was applied to the spring and the loaded natural frequencies were determined. For comparison, the unloaded natural frequencies were also found. The natural frequencies are compared in Table 3-1. For this particular example, the pre-load does not significantly alter the natural frequencies. Though this may be the case for a steel spring, this likely will not be the case for other types of mounts and materials.

The four-pole parameters were then found for the spring isolator using both the mobility and impedance matrix approaches. The lateral displacement was fixed along the center axis of the mount. The magnitudes of a_{11}, a_{12}, a_{21} and a_{22} are illustrated in Figure 3.2 to Figure 3.5.

Table 3-1 Comparison of unloaded and loaded natural frequencies.

Mode	No Pre-Load	Pre-Loaded
1	18.8	18.5
2	90.6	89.0
3	96.4	95.2
4	122.8	123.7
5	124.1	124.9
6	157.5	145.6
7	164.5	149.6
8	168.8	165.4
9	184.2	182.0
10	214.2	208.6

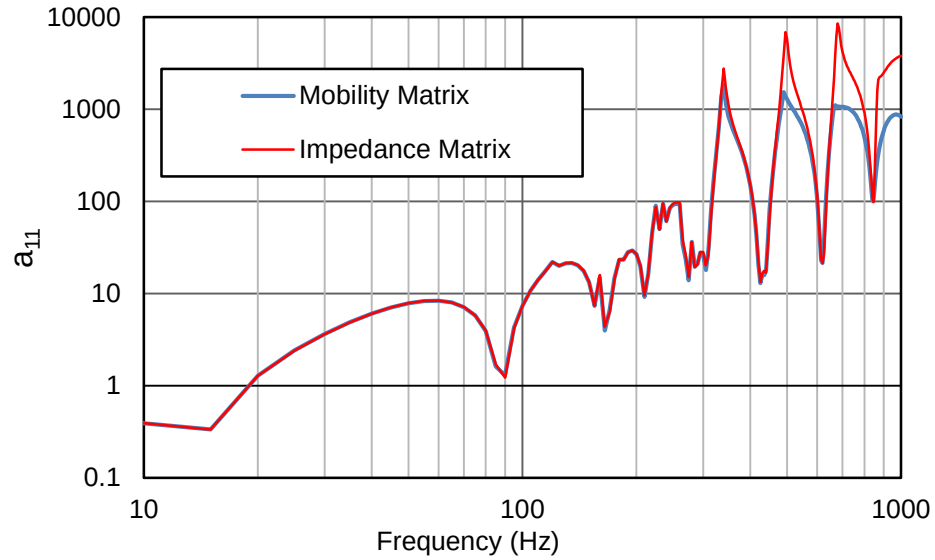

Figure 3.2 Magnitude of four-pole parameter a11 as a function of frequency.

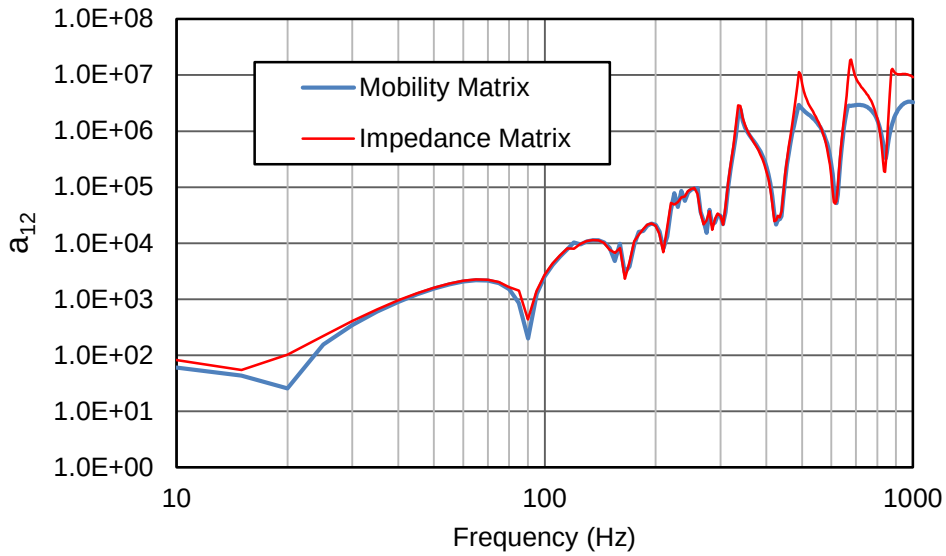

Figure 3.3 Magnitude of four-pole parameter a12 as a function of frequency.

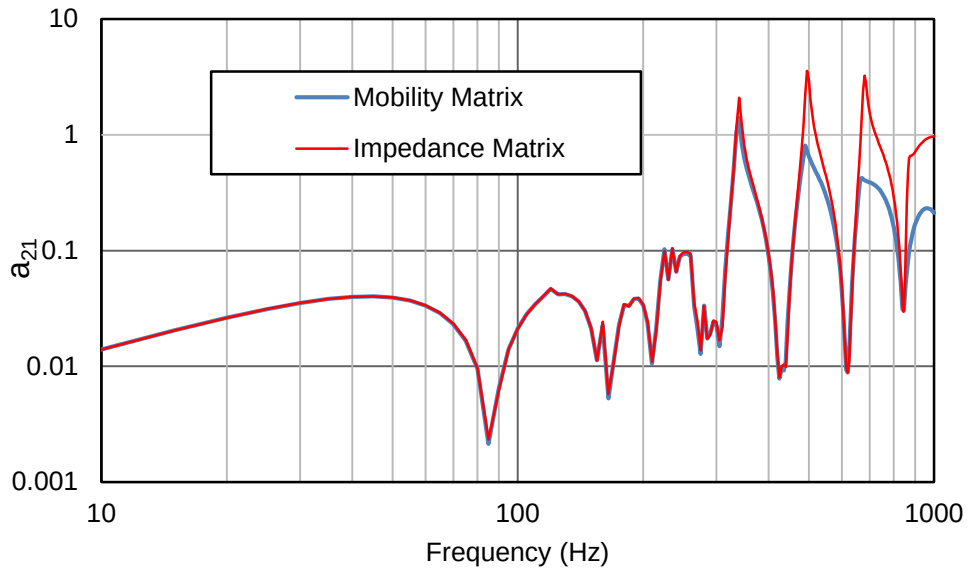

Figure 3.4 Magnitude of four-pole parameter a21 as a function of frequency.

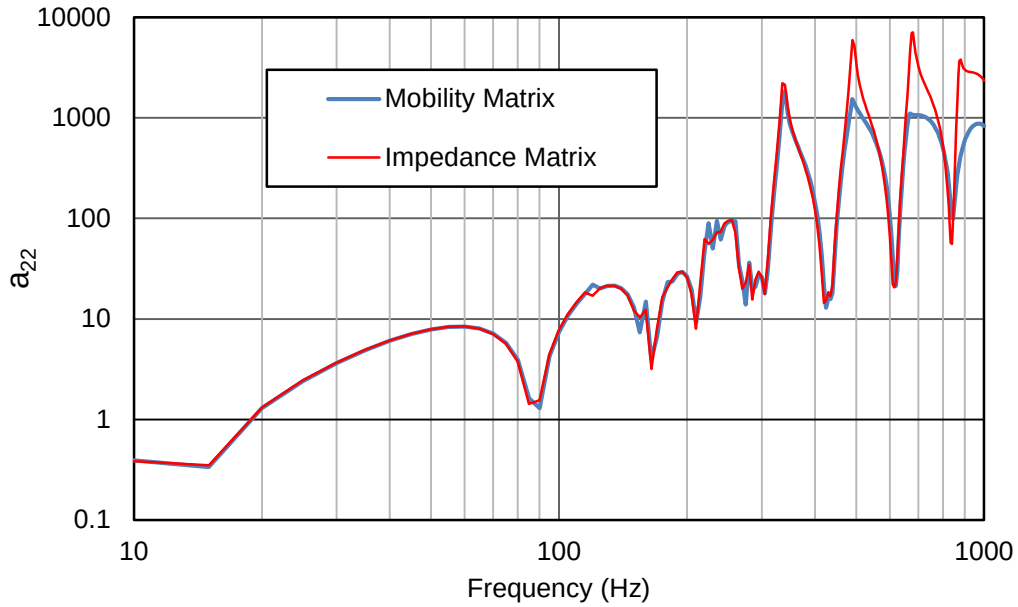

Figure 3.5 Magnitude of four-pole parameter a22 as a function of frequency.

Notice that there are some differences at higher frequencies. Though the transfer matrix parameters should be equal in theory, the difference in boundary conditions between the two approaches leads to some minor differences especially at higher frequencies. This is because the isolator end is constrained in the vertical direction when the impedance matrix approach is used which affects the rotational motion of the spring as it is compressed.

Having said that, the difference in the four pole parameters only have a minor impact on the insertion loss determined using these transfer matrices. To illustrate this point, the transfer matrices were then used to compute the insertion loss of the isolated spring placed between two plate structures. Details of the plate structures will be discussed later.

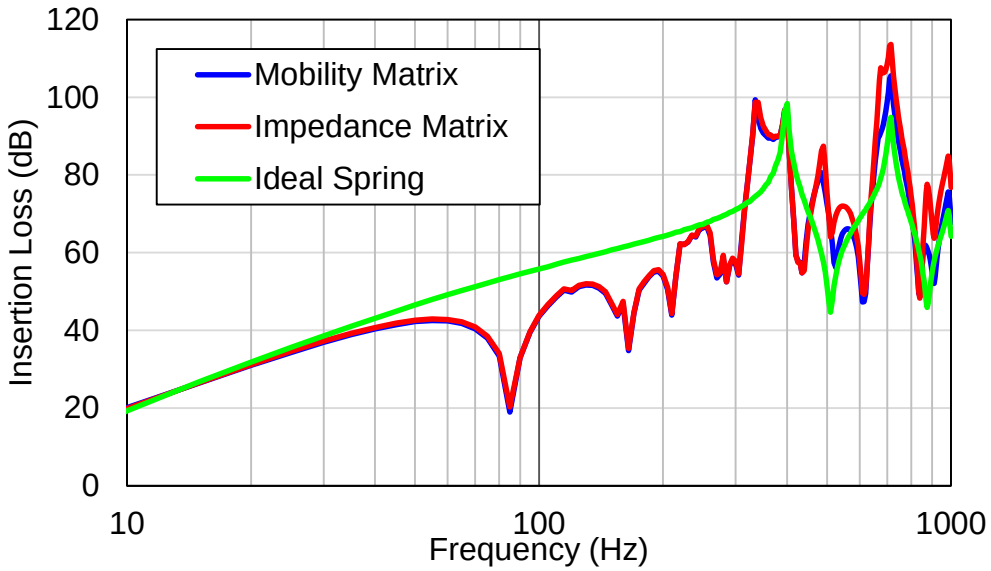

Figure 3.6 Insertion loss comparison between mobility and impedance matrix approaches with an ideal spring.

The insertion loss computed using the mobility and impedance matrix approaches are compared in Figure 3.6. The mounting frequency for the isolation system is below 10 Hz and is not shown. For the ideal spring, resonances are limited to the support structures. It is apparent that the insertion loss computed using the mobility and impedance matrix approaches captures several spring resonance frequencies that will be important if the structure is strongly excited at that particular frequency. Results compare well between the mobility and impedance matrix approaches with only minor differences at high frequencies. These differences at high frequencies are unimportant because that level of the insertion loss is unlikely to be attained in practice.

For validation purposes, the insertion loss was also compared to an FBS subtructuring calculation using LMS Virtual.Lab. The structural modes were imported from ANSYS and the system response was calculated first with an

unisolated or rigid attachment and then with the isolated connection. The isolator was modeled as a separate subsystem with transfer functions determined using finite element analysis. Insertion loss is compared in Figure 3.7 with good agreement.

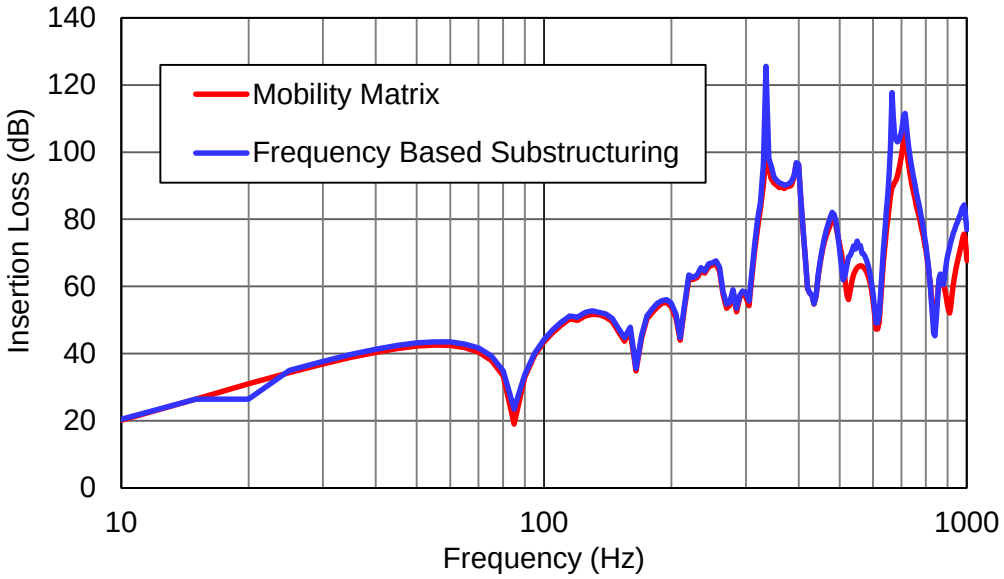

Figure 3.7 Insertion loss comparison of transfer matrix approach to frequency based substructuring.

3.5 Effect of Source and Receiver Structures

The insertion loss analysis was repeated for several different upper plate configurations. The geometry of the upper plate is shown in Figure 3.8. The upper and lower plates were assumed to be 1 cm and 5 cm thick steel respectively. The ribs shown in Figure 3.9 for the upper plate were all 1 cm thick as well. The isolator is positioned at the center of both the upper and lower plates. The source (Z_S) and receiver (Z_R) impedances were determined using finite element analysis according to equation (2.25).

Four different tests were simulated and are summarized as follows. Refer to Figure 3.9 which indicates the different configurations.

Case 1 – no ribs

Case 2 – all ribs included

Case 3 – center (orange) rib removed

Case 4 – 3 center (orange and red) ribs removed

The insertion loss is compared between the four cases in Figure 3.10. The results demonstrate the isolator insertion loss is strongly affected by the upper plate structure. In this particular case, stiffening the upper plate significantly improves the insertion loss at higher frequencies.

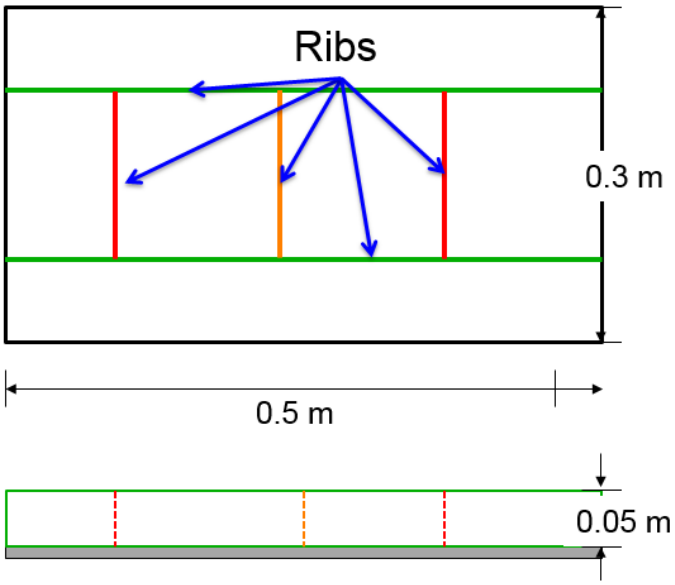

Figure 3.8 Front and top views of upper plate. All plates and ribs are 1 cm thick.

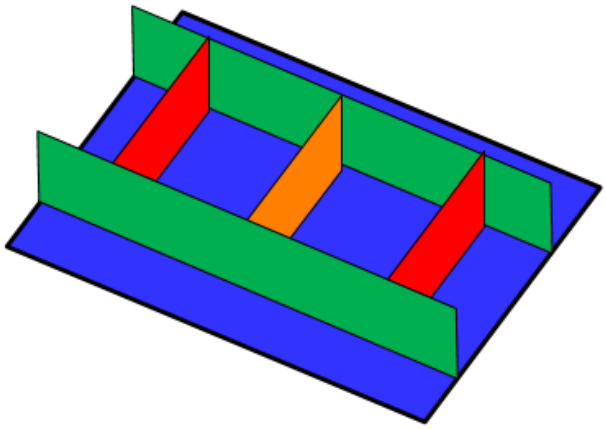

Figure 3.9 Isometric view of upper plate illustrating rib configurations.

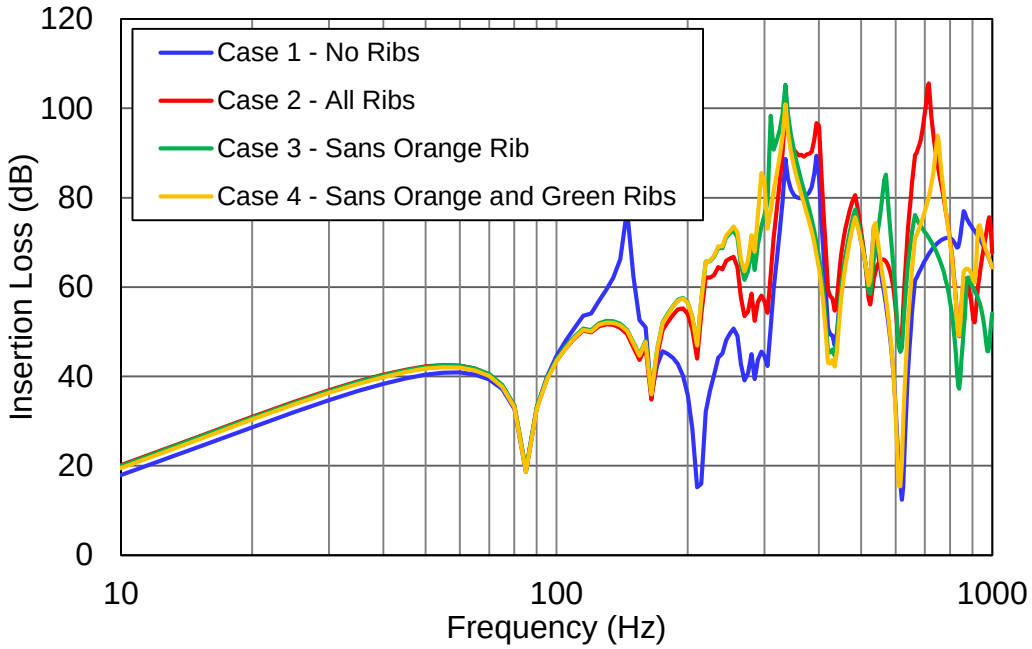

Figure 3.10 Insertion loss for different upper plate configurations.

3.6 Usefulness of Isolator Insertion Loss for Multiple Isolator Systems

The metric of isolator insertion loss seems useful for systems having a single isolator. Its suitability for systems consisting of multiple isolators is debatable. In order to investigate this question, the isolator considered in the preceding sections was used between a construction cab and base foundation in a numerical simulation study. The base foundation was a 5 cm thick baseplate, which was comparatively stiffer than the construction cab.

The construction cab was approximately 2.8 m x 1.4 m x 1.3 m. The finite element model, shown in Figure 3.11, consisted of 13,425 nodes and 11,135 elements. The model is a combination of quadrilateral and triangular shell elements, solid element, and beams. Several different materials were used for the construction cab and these materials are accordingly included in the model.

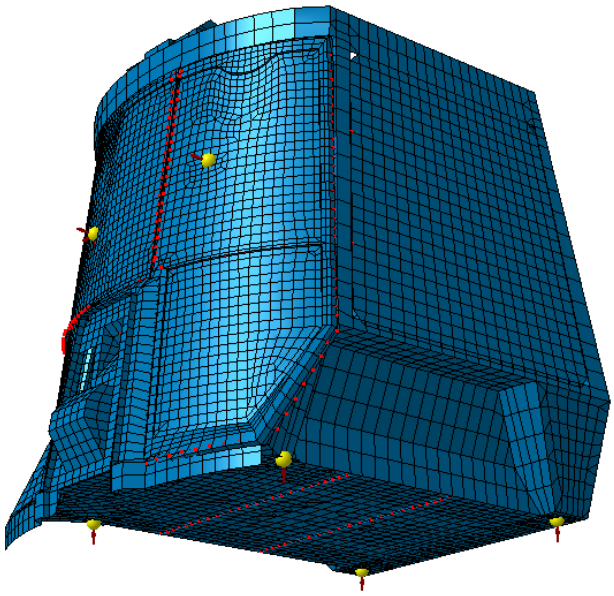

Figure 3.11 Finite element model of construction cab.

Identical isolators were assumed at each of the four corners of the construction cab in the model. For simplicity, the isolators were assumed to be the steel springs used in the earlier analyses. The source and receiver side impedances were determined using the respective finite element models and isolator insertion loss was determined using the techniques previously described.

A separate analysis was then performed to determine an insertion loss for the construction cab which includes flanking paths. In this context, flanking paths are defined as energy transmitted through the other 3 isolators. Accordingly, a finite element analysis was performed for the construction cab on four isolators with a unit force applied at the center of the base. The isolators were positioned at each of the four corners of the cab. The response was determined on the receiver or construction cab side of one of the isolators. The analysis was repeated with a rigid connection in place of the isolated connection using the same applied force. An insertion loss was determined by comparing the isolated case with that for a rigid connection. The unisolated and isolated cases are illustrated in Figure 3.12.

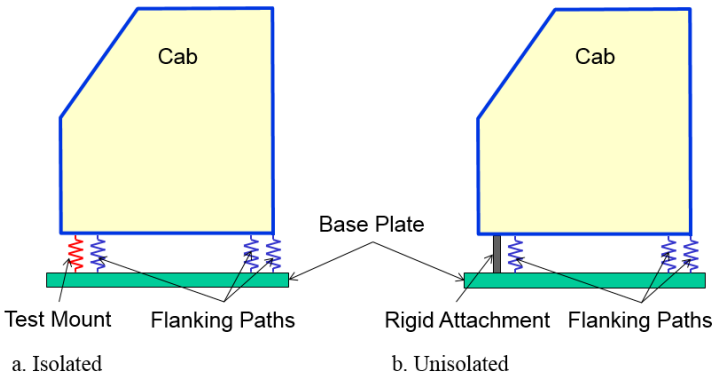

Figure 3.12 Schematic showing isolated and unisolated cases including flanking paths.

A comparison between the insertion loss determined using the transfer matrix approach and frequency based substructuring approach, which includes flanking paths, is shown in Figure 3.13. There are significant differences in the results. The results suggest that insertion loss is a questionable metric for the multiple isolator case. With that in mind, it can be seen that the isolator insertion loss approximates the average insertion loss with flanking paths included.

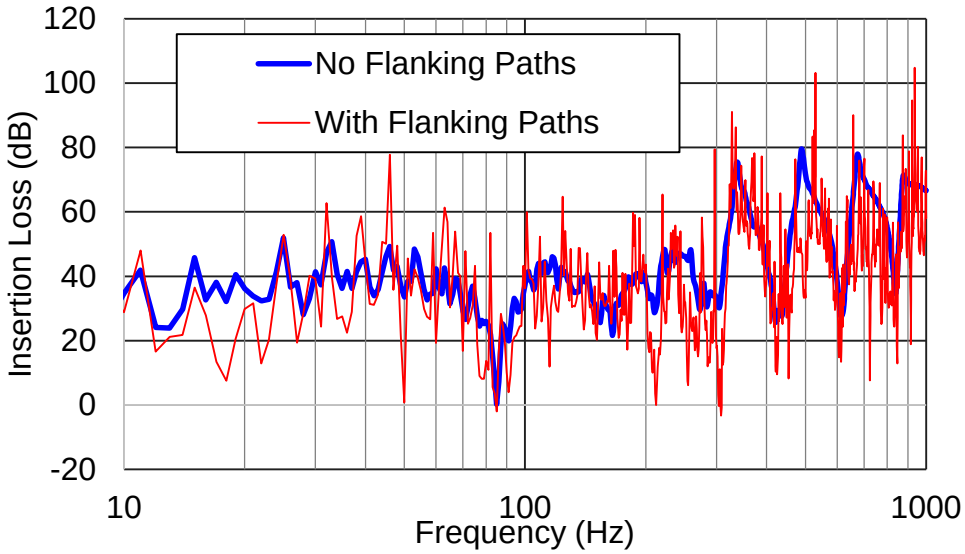

Figure 3.13 Insertion loss with and without flanking included.

3.7 Summary and Conclusions

The objective of this chapter was to review isolator transfer matrix theory and the determination of isolator effectiveness or insertion loss. It was demonstrated that the isolator transfer matrix could be determined using either mobility or impedance matrix approaches and the results were comparable between the two. The transfer matrix method for determining insertion loss was compared to direct calculation of the insertion loss using frequency based substructuring with good agreement.

It was also illustrated that insertion loss could be used to examine the effect of the attached structures. In the case examined, a spring isolator was placed between two plates. The lower plate was more massive than the upper plate. Stiffening the upper plate by adding ribs significantly improved the isolator insertion loss.

Following this, a simulation study was conducted using a construction cab attached to a flexible base through four isolation mounts. The results suggested that isolator insertion loss could be of value above the first isolator surge frequency.

This paper demonstrates a number of important concerns that noise and vibration engineers should take into consideration. It has been shown that:

- Isolator resonances will compromise the isolator performance at higher frequencies.
- Isolator performance can be predicted using finite element analysis and that results obtained using an impedance or mobility matrix approach are comparable.
- Modifications to the impedance of the connected structures at the isolator attachment points can significantly decrease the transmitted energy.
- Insertion loss is suspect as a metric particularly at lower frequencies if there are flanking paths.

CHAPTER 4 THE EFFECT OF SPRING PARAMETERS ON ISOLATOR INSERTION LOSS

4.1 Introduction

Unwanted vibration is most straightforwardly eliminated by modifications to the source. Though source vibration should be attenuated, it can rarely be altogether eliminated. In that case, it is best to introduce an impedance mismatch between the source and the structure it is mounted upon. This impedance mismatch typically takes the form of an isolator.

Isolators are typically selected based on their force or vibratory transmissibility. Transmissibility is defined as the ratio of the transmitted (F_T) to the input force (F_0) or vibration. Though force and vibration applications are very different, the transmissibility ratio ($T.R.$) is identical for either case. The force transmissibility can be expressed as

$$T.R. = \frac{F_T}{F_0} = \sqrt{\frac{1 + (2\zeta r)^2}{(1 - r^2)^2 + (2\zeta r)^2}} \tag{4.1}$$

Where ζ is the viscous damping ratio. r is the ratio ω/ω_n where ω is the forcing frequency and ω_n is the mounted resonance frequency which typically falls quite low in frequency (below 10 Hz). Notice that Equation (4.1) depends on the damping and mounted or first resonant frequency of the isolator system.

Inman (2001) ably describes a process for selecting isolators. After noting the input frequency and desired reduction in force at that particular frequency, the designer can select an appropriate static deflection. The spring stiffness (k) is then determined from the static deflection and the mass of the isolated machine. This selection process is commonly abetted by use of design curves. For engines and heavy equipment, coiled springs have been preferred since they permit the necessarily large static deflection and are relatively small in size (Inman, 2001).

The methodology introduced so far does not take into account the compliance of the machine or foundation which reduces the isolator effectiveness. Of greater importance, the isolator itself will have resonant frequencies sometimes referred to as surge frequencies which further compromise the performance of the isolator (Wallin et al., 2011).

At higher frequencies, the metric most commonly used to assess isolator performance is insertion loss. Insertion loss is defined as the difference in dB between the vibration if the machine and foundation are rigidly attached compared to the isolated case. Insertion loss takes into account the compliance on the machine and foundation sides of the isolator. Figure 4.1 illustrates the effect of wave propagation in the isolator (compliance of the machine and foundation are included). The insertion loss of an isolator is decreased significantly particularly at the first surge frequency (around 90 Hz) and at subsequent resonant frequencies.

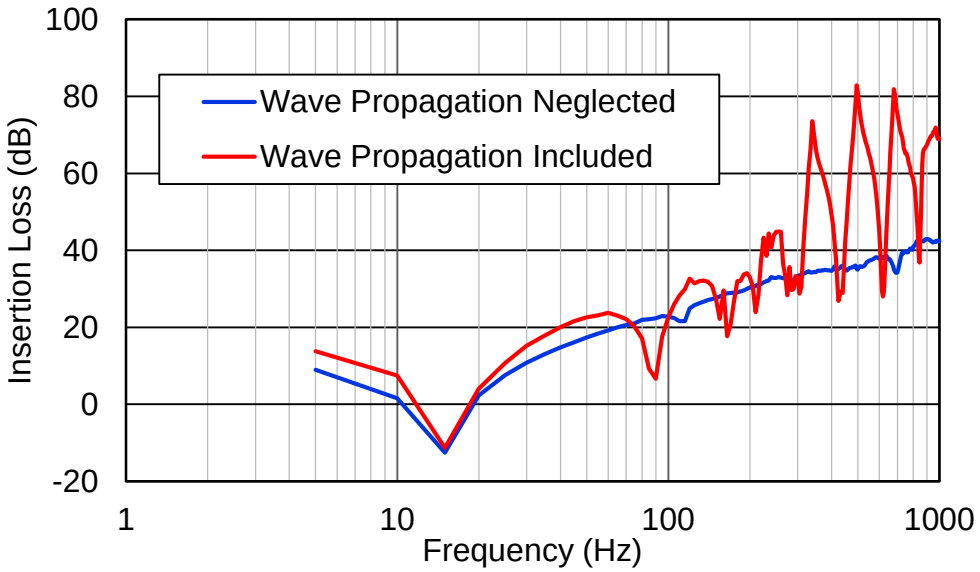

Figure 4.1 Insertion loss of spring isolator neglecting and including wave propagation in the isolator.

Determination of insertion loss depends on first identifying the transfer matrix of the isolator and knowing the impedance on both the source and receiver sides of

the isolator. In the current work, the transfer matrix of an isolator is determined using finite element analysis. A static analysis is first performed to establish the isolator preload. This is followed by a modal and then a modal superposition forced response analysis.

The current chapter is focused on spring isolators like those commonly used in heavy equipment, automotive, and HVAC applications. The effect of different spring parameters on the insertion loss and first surge frequency of a spring isolator is examined. The objective of the chapter is to give the reader some confidence in using predictive tools to examine the high frequency performance of isolators as well as providing some intuition on how modifications to a spring isolator impact high frequency performance.

4.2 Determination of the Insertion Loss

When determining the insertion loss of an isolator, it is first expedient to identify the transfer matrix, suggested by Molloy (1957) and Snowdon (1971), which relates forces and velocities on the source and foundation sides of the isolator. The force and vibration on the machine or source (F_1 and v_1) and foundation or receiving (F_2 and v_2) sides can be expressed via the matrix Equation (2.11), where a_{11}, a_{12}, a_{21}, and a_{22} are complex and frequency dependent.

Dickens and Norwood (1994, 1995, 2001) determined the transfer matrix terms a_{11}, a_{12}, a_{21}, and a_{22} via measurement. However, the transfer matrix terms are most easily determined using analysis. In Chapter 3, the transfer matrix was determined using mobility and impedance matrix approaches. The latter is adopted here.

The impedance matrix can be expressed as Equation (3.12), where c_{11}, c_{12}, c_{21}, and c_{22} are the respective impedance matrix terms. Two successive forced response analyses are required to determine matrix terms. The boundary

conditions for the first and second analysis are shown in Equations (3.13) and (3.14) respectively. Once the impedance matrix terms (c_{11}, c_{12}, c_{21}, and c_{22}) are determined, the transfer matrix can be expressed as

$$\begin{bmatrix} a_{11} & a_{12} \\ a_{21} & a_{22} \end{bmatrix} = \begin{bmatrix} c_{11}/c_{21} & c_{12} - c_{11}c_{22}/c_{21} \\ 1/c_{21} & -c_{22}/c_{21} \end{bmatrix} \tag{4.2}$$

Isolator insertion loss compares the dB difference between unisolated and isolated responses and is mathematically expressed as

$$IL = 20\log_{10}\left(\frac{\left|v_f^{\text{rigid}}\right|}{\left|v_f^{\text{isolated}}\right|}\right) \tag{4.3}$$

where $v_f^{\text{rigid}}$and v_f^{isolated} are the unisolated and isolated responses respectively. The insertion loss can be written as Equation (2.47), where Z_S and Z_R are the mechanical impedances on the machine and foundation sides respectively.

4.3 Finite Element Analysis Approach

All analyses were performed using ANSYS Workbench. The analysis process was comprised of 3 steps. 1) A static finite element analysis was performed to pre-load the isolator and account for stress stiffening effects. In Chapter 3, it was demonstrated that stress stiffening effects only have a minimal influence on the determined structural modes (Sun, 2015). 2) This is followed by a structural modal analysis to determine the structural modes of the isolator. 3) Afterwards, modal superposition forced response analyses are performed to determine the transfer matrix of the isolator as described in the prior section. A steel spring is assumed for all analyses. Hence, the elastic modulus, mass density and Poisson's ratio are 200 GPa, 7800 kg/m^3, and 0.3 respectively.

4.4 Parametric Sensitivity Study

A sensitivity study was performed to examine the effect of changing various geometric quantities for a steel spring. A schematic of a typical steel coiled spring is illustrated in Figure 4.2. The variables of interest are the wire diameter (d), the spring diameter (D), the height of the spring (H) and the number of active coils (n).

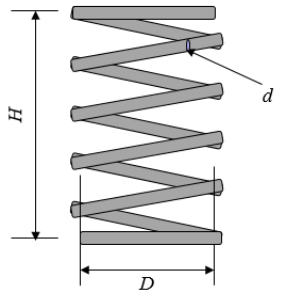

Figure 4.2 Schematic showing geometric variables of interest for a steel spring.

In any spring, some portion of the end coils will probably be inactive. The number of the inactive coils varies depending on the spring end configuration and mating component geometry.

Springs can be coiled with a variety of end configurations. If the space between the coils is reduced to the point where the wire at the tip makes contact with the next coil, the end is said to be “closed”. If there is no reduction in pitch at the end coils, the end is referred to as “open”. Between these two extremes is an end type known as “semi-closed” in which the space between coils is reduced, but there is a gap between the tip and next coil. The most common configuration in industrial springs is closed ends. Four end types are illustrated in Figure 4.3, from left to right, it is (a) plain; (b) plain and ground; (c) squared; (d) square and ground. Table 4-1 shows the equations used to define the ends coils and active coil turns for those four different end types (Schmid, 2013). Where N_t is the total

number of coil turns. It should be noted that for the simulation cases performed in this work, all the spring ends is the plain and ground type.

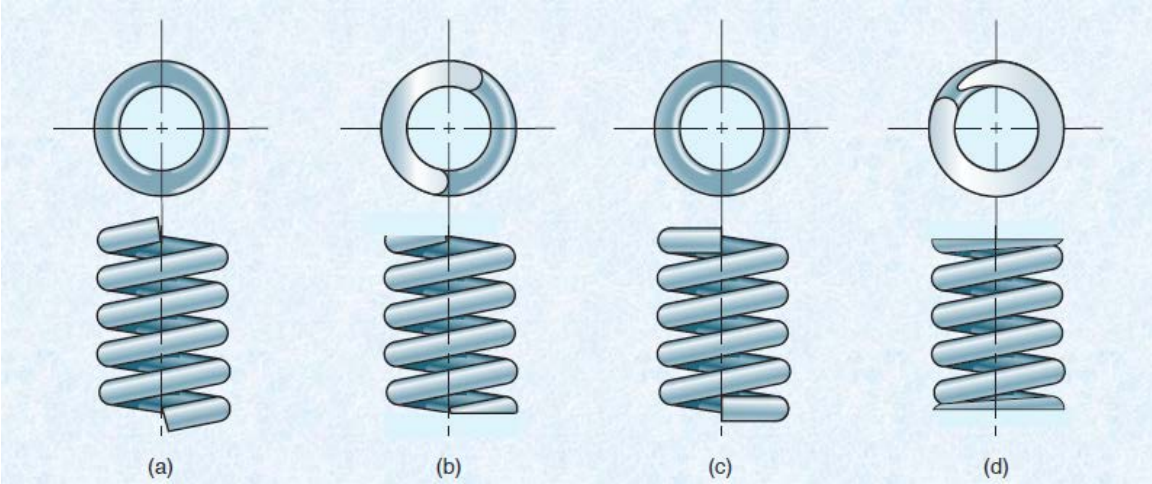

Figure 4.3 Four end types commonly used in compression springs (Schmid, 2013).

Table 4-1 Compression spring coil equations.

	Type of spring end			
Term	Plain	Plain and ground	Squared or closed	Squared and ground
Number of end coils, n_e	0	1	2	2
Total number of active coil turns, n	N_t	$N_t - 1$	$N_t - 2$	$N_t - 2$

The stiffness of a spring can be estimated (Ungar, 2007) using Equation (3.27), where G is the shear modulus, d is the spring wire diameter, D is the diameter of

the spring, and n is the number of active turns. The mass of the spring can be estimated via

$$m = \frac{\rho \pi d^2}{4} \sqrt{(n\pi D)^2 + H^2} \tag{4.4}$$

where ρ is the mass density of the spring.

If it is assumed that 1) the mass of the isolator is much smaller than that of the machine and foundation and 2) the damping is low, the spring stiffness largely determine the insertion loss at low frequencies and at non-resonant frequencies. From Equations (2.47) and (3.27), it can be shown that

$$IL \propto 20 \log_{10} \left| \frac{\omega 8 n D^3}{G d^4} \right| \tag{4.5}$$

From examining the mode shapes, it was observed that the first surge mode of the isolator is a longitudinal mode where the center of the spring oscillates back and forth. In a very approximate sense, the mode can be considered as a mass in between two springs. Accordingly, the mode can be approximated as the $\sqrt{k/m}$ where k and m are defined in Equations (3.27) and (4.4) respectively. In that case, a proportionality relationship for the first surge frequency (f_1) can be expressed as

$$f_1 \propto \frac{d}{nD^2} \sqrt{\frac{G}{2\pi\rho}} \tag{4.6}$$

4.4.1 Effect of Spring Diameter

The effect of spring diameter (D) was examined. The wire diameter (d) was 5 mm, height (H) is 7.5 cm, and the number of active turns (n) was approximately 3.5. The isolator was placed in between masses of 10 and 100 kg respectively and the insertion loss was determined using Equation (2.47). The damping of the isolator was assumed to be 0.001 which is unreasonably low. This allowed for the first surge frequency to be identified easily from the plots.

The spring diameter was varied and results are shown in Figure 4.4. If results are examined at 20 Hz, the increase in insertion loss gained by increasing the spring diameter from 3 cm to 5 cm and 7 cm is 11 and 19 dB respectively. Using the proportionality relationship in Equation (4.5), the predicted increase in insertion loss is 13 and 22 dB respectively. It can be seen that the proportionality relationship provides a rough estimate of the increase in insertion loss.

Based on the proportionality relationship in Equation (4.6), the ratio of the surge frequencies between 9 cm and 7 cm, 7 cm and 5 cm, and 5 cm and 3 cm is anticipated to be 1.7, 2.0, and 2.8 respectively. The finite element analysis shows that the actual ratios are 1.8, 2.1, and 2.5 respectively. It can be seen that the proportionality relationship reliably estimates the change in the surge frequency.

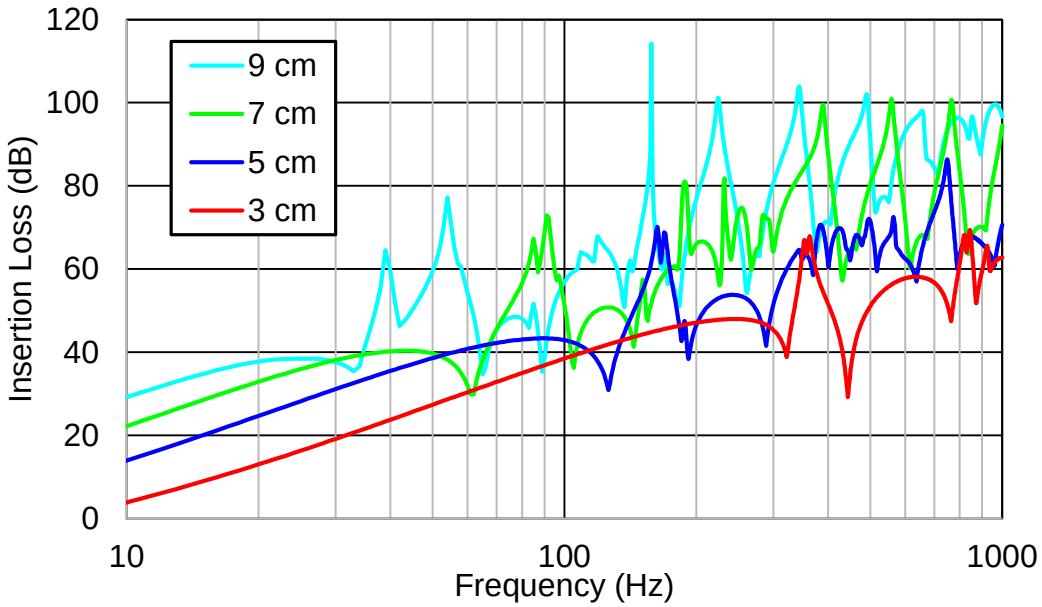

Figure 4.4 Insertion loss of steel spring with varying spring diameter.

4.4.2 Effect of Wire Diameter

The effect of spring diameter was examined next. The spring diameter (D) was 7 cm, height (H) is 7.5 cm, and the number of active turns (n) was approximately 3.5. Insertion loss results are shown in Figure 4.5. The insertion loss was again compared at 20 Hz. Based on Equation (4.5), the increase in insertion loss due to reducing the wire diameter from 1.5 cm to 1 cm and from 1 cm to 0.4 cm is predicted to be 14.1 dB and 31.8 dB respectively. This compares well with the finite element simulation predictions of 11.0 dB and 40.6 dB.

Based on Equation (4.6), the ratios of the surge frequencies between 1.0 cm and 0.4 cm and 1.5 cm and 1.0 cm is anticipated to be 2.5 and 1.5 respectively. Finite element simulation predicts the ratios to be 2.9 and 1.7 respectively. Though there is some difference, the proportionality relationship provides a rough estimate of the change in the surge frequency.

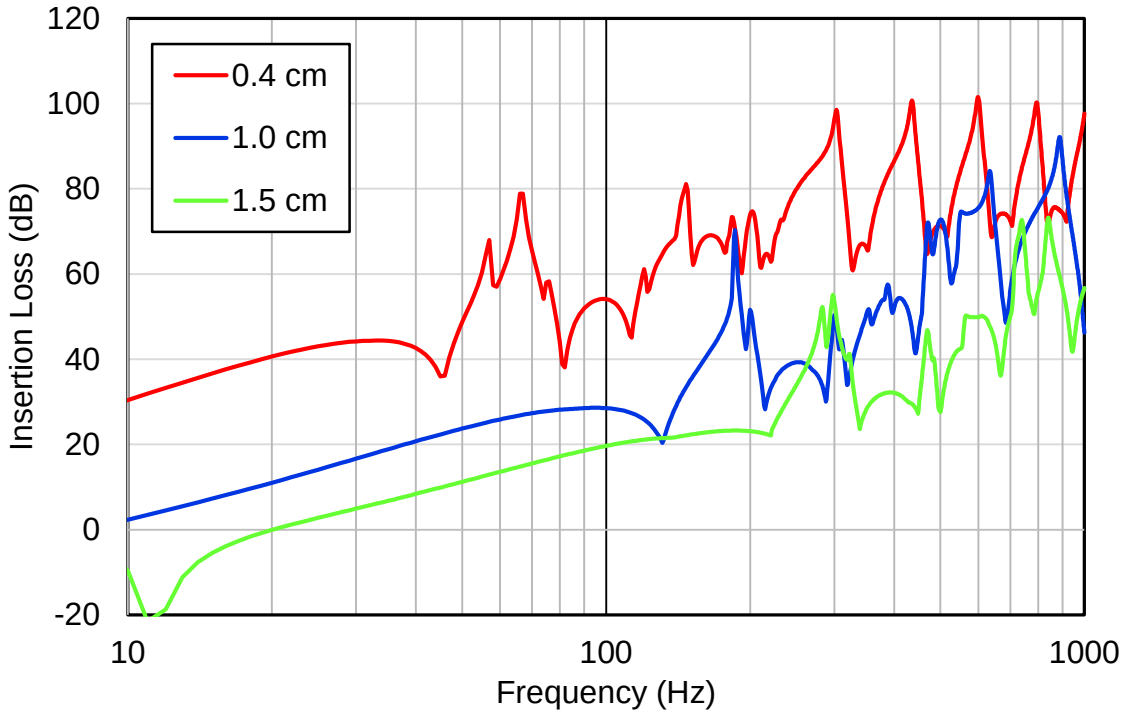

Figure 4.5 Insertion loss of steel spring with varying wire diameter.

4.4.3 Effect of Number of Active Turns

The number of active turns is subjective. For the cases considered, the first turn on each side of the isolator was assumed inactive, and hence, neglected. Figure 4.6 shows the insertion loss for 3.5 and 7 active turns. The wire diameter (d) is 5 mm, spring diameter (D) is 7 cm, and height (H) is 7.5 cm. According to Equation (4.5), the insertion loss is expected to increase by 6 dB for a doubling of the number of turns. The finite element simulation indicates a 4.2 dB increase at 10 Hz. The ratio of the surge frequency is anticipated to be 2.0 whereas the analysis reveals it to be 1.8.

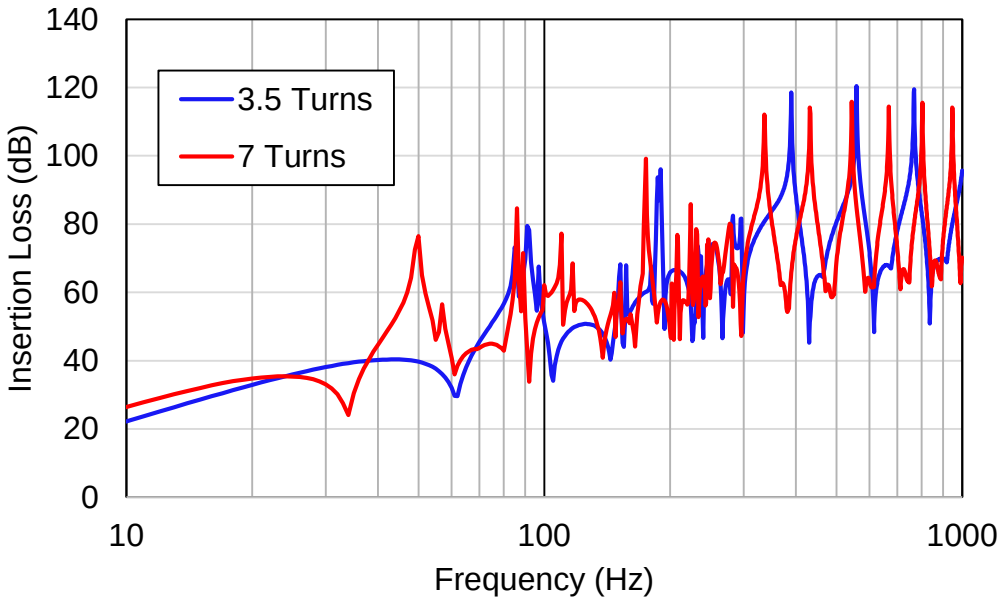

Figure 4.6 Insertion loss of steel spring with varying number of active turns.

4.4.4 Effect of Source and Foundation Compliance

The isolator was then positioned between compliant machine and foundation plates. The finite element models for the machine and foundation plates are shown in Figure 4.7. The machine and foundation plates were assumed to be 1 cm and 5 cm thick steel respectively. The upper plate is ribbed and is shown in Figure 4.7. The ribs are all 1 cm thick. The isolator is positioned at the center of both the upper and lower plates. The machine (Z_S) and foundation (Z_R) impedances were determined using finite element analysis.

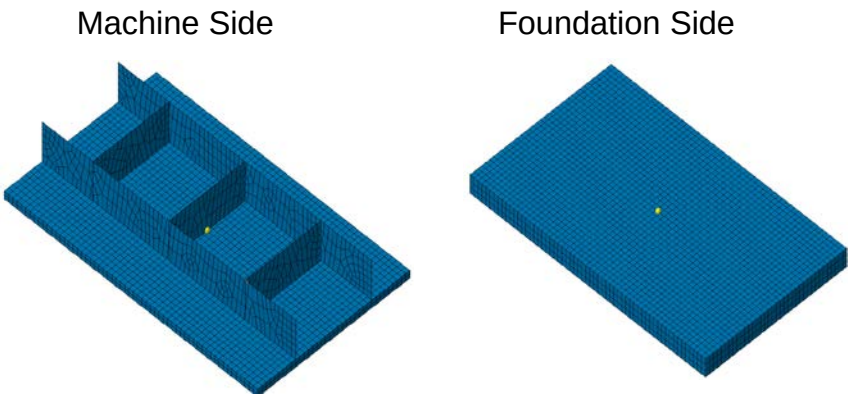

Figure 4.7 Finite element models of the machine and foundation sides.

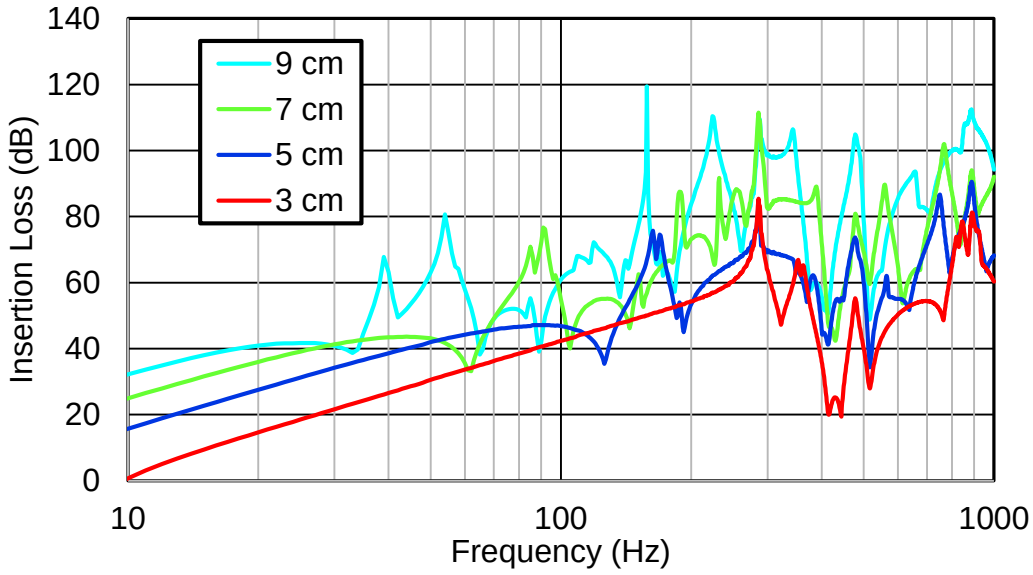

Figure 4.8 Insertion loss with compliant machine and foundation for varying spring diameter.

In Figures 4.8 and 4.9, the insertion loss for varying spring and wire diameters are plotted respectively. It can be observed that the trends are very similar to those that were observed in Figures 4.4 and 4.5 where the machine and foundation sides were modeled as simple masses. Notice that the effect on insertion loss and surge frequency is nearly the same. The primary differences are that there are some additional resonances due to the machine and foundation. Otherwise, insertion loss and surge frequencies are similar.

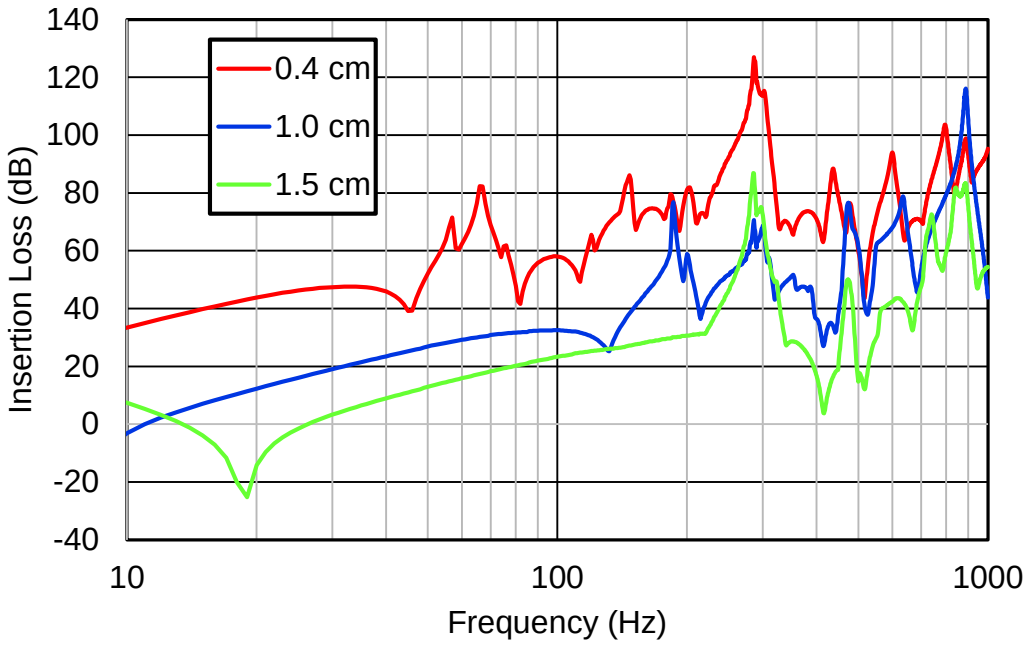

Figure 4.9 Insertion loss with compliant machine and foundation for varying wire diameter.

4.5 Summary

Insertion loss is commonly used as a metric to characterize the high frequency performance of a spring isolator. A simple sensitivity study was performed to examine the effect of varying geometric parameters on the insertion loss and the first surge frequency for a simple coiled spring isolator. The results were shown to correlate well with some expected proportionality relationships which correlate insertion loss and the first surge frequency to the spring diameter, wire diameter, and number of active turns. The results were shown to be extendable to the case of a spring isolator with compliant source and foundation.

CHAPTER 5 SUMMARY AND RECOMMENDATION

5.1 Summary

When a wave propagating in an elastic medium meets an abrupt change in impedance, only part of the wave passes through the discontinuity. The remaining portion of the wave is reflected back towards the direction from which the incident wave arrives. In the case of vibration isolation, one seeks to hinder the propagation of the wave by introducing such discontinuities in properties along the propagation path. The most common way is to incorporate an element that is considerably more compliant, i.e., has a lower stiffness than that of the surrounding medium. Such an element is usually called a vibration isolator. Since common materials used in machines and vehicles are relatively stiff, it is often simpler to obtain significant discontinuities in the properties by using a compliant element.

Several different rules of thumb should be followed when using isolation. First of all, the mounting positions should generally be as stiff as possible since compliance at the attachment points generally compromises isolator performance. Secondly, the isolator's stiffness should be selected so that that the mounted frequency is well below the lowest excitation frequency of concern. Thirdly, the operating speed of the machinery should be controlled so it will pass through the lowest excitation frequency quickly. Fourthly, the total system resonances should be determined and avoided if possible. Adding stiffening ribs can increase component resonances. After all these measures are taken, it is often found that wave propagation within the isolator will compromise the isolator performance at higher frequencies.

The metric most often used to assess the performance of an isolator at high frequencies is the insertion loss. Insertion loss is defined as the difference in decibels between the vibration on the receiver side for the rigidly attached and the isolated cases. The research presented in this thesis looks at the development of a simulation approach to determine the insertion loss of an isolator installed between two components. The first step in doing so is to

determine the transfer matrix for the isolator. The isolator transfer matrix was determined using both mobility and impedance matrix approaches and insertion loss results were shown to be comparable between the two approaches. For further verification, the transfer matrix method for determining insertion loss was compared to direct calculation using frequency based substructuring with good agreement.

It was also illustrated that the effect of the mounted impedances could be assessed and incorporated in the model. An example was considered where a spring isolator was placed between two plate structures. The lower plate, considered the receiver, was more massive than the upper plate. Stiffening the upper plate by adding ribs improved the isolator insertion loss at high frequencies.

Further simulation work examined the case of a construction cab attached to a flexible base through four isolation mounts. When flanking paths are included, insertion loss was shown to have limited value. Accordingly, insertion loss is most appropriate for the single isolator case and likely has limited value when several isolators are used.

Following this, the research looked at the insertion loss of spring isolators. The geometric parameters which effect the insertion loss and first surge frequency are the spring diameter, wire diameter and number of active turns. Simple proportionality relationships were developed to explain the effect of each of the aforementioned geometric parameters on both the insertion loss and the first surge frequency. These relationships should prove useful for diagnostic purposes when changes need to be made to modify the first surge frequency without adversely affecting the insertion loss.

5.2 Recommendations

Several recommendations for future work can be made based on the research presented in this thesis. These include the following.

1. An insertion loss test rig should be developed to validate the proportionality relationships developed for spring isolators.
2. Models should be developed for more realistic isolators which include elastomer layers, and embedded masses.
3. The mobility and impedance matrix approach should be further developed and validated for multi-dimensional characterization of vibration isolators.
4. The applicability of extending the transfer matrix approach to continuous vibration systems should be examined
5. The cases of multiple mount systems should be examined with a goal towards establishing appropriate metrics.
6. Rubber mount stiffness and damping should be investigated and evaluated.

Appendix

This section is to show the complete and detailed equations for isolator parametric sensitivity used in the Chapter 4.

The spring mass m can be found by the spring volume and its material density, which is expressed as

$$m = \rho \cdot Vol = \rho \cdot \left(\frac{d}{2}\right)^2 \pi \cdot L_{wire} \tag{A.1}$$

where ρ is the density of the material, d is the spring wire diameter and L_{wire} is the wire length, and can be calculated from the length of coils of the spring and the height of the spring, which is given as

$$L_{wire} = \sqrt{(n\pi D)^2 + H^2} \tag{A.2}$$

where D is the spring diameter, H is the height of the spring, and n is the number of active turns. Then substitute equation (A.2) to equation (A.1), the mass of the spring can be estimated via

$$m = \frac{\rho \pi d^2}{4} \sqrt{(n\pi D)^2 + H^2} \tag{A.3}$$

If it is assumed that 1) the mass of the isolator is much smaller than that of the machine and foundation and 2) the damping is low, the spring stiffness largely determines the insertion loss at low frequencies and at non-resonant frequencies. From Equations (2.47) and (3.27), it can be shown that

$$IL \propto 20 \log_{10} \left| j \frac{\omega}{k} \right| = 20 \log_{10} \left| \frac{\omega 8 n D^3}{G d^4} \right| \tag{A.4}$$

From examining the mode shapes, it was observed that the first surge mode of the isolator is a longitudinal mode where the center of the spring oscillates back and forth. In a very approximate sense, the mode can be considered as a mass in between two springs. Accordingly, the mode can be approximated as the

$\sqrt{k/m}$ where k and m are defined in Equations (3.27) and (4.4) respectively. In terms of the mass, if the magnitude of spring diameter and spring height are on the same order, (normally the wire length will be relatively long compared to the spring height) then the terms $(n\pi D)^2$will be very large compared to the term H^2 and it will be dominant. In that case, a proportionality relationship for the first surge frequency (f_1) can be expressed as

$$f_1 \propto \frac{d}{nD^2}\sqrt{\frac{G}{2\pi\rho}} \tag{A.5}$$

REFERENCES

ANSYS 14.0 Workbench, Academic Research, 2014.

J. D. Dickens and C. J. Norwood, (1994). “Measurement of Four-Pole Parameters using Floating Masses,” Australian Acoustical Society Annual Conference, pp. 57-65.

J. D. Dickens and C. J. Norwood, (1995). “Measurement of Four-Pole Parameters using Direct Forces,” Australian Acoustical Society Annual Conference, pp. 15-21.

J. D. Dickens, (1998). “Dynamic Characterization of Vibration Isolators,” Ph. D. Thesis, The University of New South Wales, Australia.

J. D. Dickens, (2000). “Dynamic Model of Vibration Isolator under Static Load,” Journal of Sound and Vibration, Vol. 236, pp. 323-337.

J. D. Dickens, (2000). “Methods to Measure the Four-Pole Parameters of Vibration Isolators,” Acoustics Australia, Vol. 28, pp. 15-21.

J. D. Dickens and C. J. Norwood, (2001). “Universal Method to Measure Dynamic Performance of Vibration Isolators under Static Load,” Journal of Sound and Vibration, Vol. 244, pp. 685-696.

J. A. Forrest, (2006). “Experimental modal analysis of three small-scale vibration isolator models,” Journal of Sound and Vibration, Vol. 289, pp. 382-412.

P. Gardonio and S. J. Eliott, (2000). “Passive and active isolation of structural vibration transmission between two plates connected by a set of mounts,” Journal of Sound and Vibration, Vol. 237, pp. 483-511.

W. Hendricx and D. Vandenbroeck, (1993). “Suspension Analysis in View of Road Noise Optimization,” SAE Technical Paper No. 931343.

D. W. Herrin, J. Liu and G. Sampath, (2009). “The applicability of the Mobius transformation to mechanical and acoustic impedance modifications,” Journal of Sound and Vibration, Vol. 328, pp. 382-395.

D. J. Inman, (2001). Engineering Vibration, Chapter 5, Second Edition.

ISO 10846-1, (1997). “Acoustics and Vibration－Laboratory measurement of vibro-acoustic transfer properties of resilient elements－Part 1: Principles and guidelines.”

ISO 10846-2, (1997). “Acoustics and Vibration－Laboratory measurement of vibro-acoustic transfer properties of resilient elements－Part 2: Dynamic stiffness of elastic supports for translator motion－Direct method.”

ISO 10846-3, (2002). “Acoustics and Vibration－Laboratory measurement of vibro-acoustic transfer properties of resilient elements－Part 3: Indirect method for determination of the dynamic stiffness of resilient supports for translator motion.”

ISO 10846-4, (2002). “Acoustics and Vibration－Laboratory measurement of vibro-acoustic transfer properties of resilient elements－Part 4: Dynamic stiffness of elements other than resilient supports for translatory motion.”

G. D. Izak, (1993). Noise and Vibration Control in Vehicles, Chapter 5, M. J. Crocker and N. I. Ivanov, Politekhnika, St. Petersurg.

M. H. A. Janssens, J. W. Verheij and D. J. Thompson, (1999). “The Use of an Equivalent Forces Method for the Experimental Quantification of Structural Sound Transmission in Ships,” Journal of Sound and Vibration, pp. 305-328.

S. Kim and R. Singh, (2001). “Multi-Dimensional Characterization of Vibration Isolators over a Wide Range of Frequencies,” Journal of Sound and Vibration, Vol. 245, pp. 877-913.

S. Kim and R. Singh, (2003). “Examination of Some Vibration Isolator Models and Their Effects on Vibration and Structure-borne Noise Transmission,” SAE Technical Paper No. 2003-01-1477.

T. C. Lim and G. C. Steyer, (1992). “System Dynamics Simulation Based on Structural Modification Analysis Using Response Techniques,” Tenth International Modal Analysis Conference, San Diego, pp. 1153-1158.

P. J. G. van der Linden and J. K. Fun, (1993). “Using Mechanical-Acoustical Reciprocity for Diagnosis of Structure-Borne Sound in Vehicles,” SAE Technical Paper No. 931340.

LMS Virtual. Lab, Siemens AG, 2014.

C. T. Molloy, (1957). “Use of Four-Pole Parameters in Vibration Calculations,” Journal of the Acoustical Society of America, Vol. 29, pp. 842-853.

M. L. Munjal, (1987). Acoustic of Duct and Mufflers, John Wiley, New York (1987).

C. J. Norwood, (1987). “Vibration isolator properties and performance prediction,” Odegaard & Danneskiold-Samsoe report no. 87.199, Copenhagen.

C. J. Norwood and J. D. Dickens, (1998). “The Effect of Vibration Isolator Properties and Structural Stiffness on Isolator Performance,” Journal of Vibration and Control, 1998 4: 253.

F. Schloss, (1965). “Recent Advances in Mechanical Impedances Instrumentation and Applications,” U.S. Navy David Taylor Model Basin, no. 1960, Washington.

S. R. Schmid, B. J. Hamrock and B. O. Jacobson, (2013). Fundamentals of Machine Elements, Third Edition, CRC Press.

J. C. Snowdon, (1961). “Reduction of the response to vibration of structures possessing finite mechanical impedance,” Journal of the Acoustical Society of America, 33, 1466.

J. C. Snowdon, (1965). “Rubberlike Materials, Their Internal Damping and Role in Vibration Isolation,” Journal of Sound and Vibration, Vol. 2, pp. 175-193.

J. C. Snowdon, (1968). Vibration and Shock in Damped Mechanical System, John Wiley and Sons, New Tork (1968).

J. C. Snowdon, (1971). “Mechanical Four-Pole Parameters and Their Application,” Journal of Sound and Vibration, Vol. 15, pp. 307-323.

J. C. Snowdon, (1979). “Vibration Isolation: Use and Characterization,” Journal of the Acoustical Society of America, Vol. 66, pp. 1245-1274.

J. I. Soliman and M. G. Hallam, (1968). “Vibration isolation between non-rigid machines and non-rigid foundations,” Journal of Sound and Vibration, Vol. 8, pp. 329-351.

S. Sun, D. Herrin and J. Baker, (2015). “Determination of the Transfer Matrix for Isolators Using Simulatoin with Application to Determining Insertion Loss,” SAE Technical Paper 2015-01-2226.

E. E. Ungar and C. W. Dietrich, (1966). “High Frequency Vibration Isolation,” Journal of Sound and Vibration, Vol. 4, pp. 224-241.

E. E. Ungar, (2007). Handbook of Noise and Vibration Control, Chapter 59, M. J. Crocker, John Wiley and Sons, New Jersey, pp. 1186-1196.

J. W. Verheij, (1982). “Multi-path sound transfer from resiliently mounted shipboard machinery: Experimental methods for analyzing and improving noise control,” Ph. D. Thesis.

D. de Vis, W. Hendricx and P. J. G. van der Linden, (1992). “Development and Integration of an Advanced Unified Approach to Structure Borne Noise Analysis,” Second International Conference on Vehicle Comfort, ATA.

H. P. Wallin, U. Carlsson, M. Åbom, H. Bodén and R. Glav, (2012). Sound and Vibration, Marcus Wallenberg Laboratoriet.

K. Wyckaert and H. Van der Auweraer, (1995). “Operational Analysis, Transfer Path Analysis, Modal Analysis: Tools to Understand Road Noise Problems in Cars,” SAE Technical Paper No. 951251.

VITA

Shishuo Sun was born in Qingdao, China in 1987. He received the Bachelor's degree of Science in Mechanical Engineering and Automation from Qingdao University of Science & Technology, China in 2011. In August 2012, he enrolled in Department of Mechanical Engineering at University of Kentucky, for graduate study and research assistant. He had two conference papers published on SAE International. He had a Summer Internship opportunity at Cummins Power Generation in 2015. He joined Nelson Global Products, as a full time NVH Development Engineer since September 2015.